

MIT Open Access Articles

Preheating after multifield inflation with nonminimal couplings. II. Resonance structure

The MIT Faculty has made this article openly available. **Please share** how this access benefits you. Your story matters.

Citation: DeCross, Matthew P. et al. "Preheating after multifield inflation with nonminimal couplings. II. Resonance structure." *Physical Review D* 97, 2 (January 2018): 023527 © 2018 American Physical Society

As Published: <http://dx.doi.org/10.1103/PhysRevD.97.023527>

Publisher: American Physical Society

Persistent URL: <http://hdl.handle.net/1721.1/115537>

Version: Final published version: final published article, as it appeared in a journal, conference proceedings, or other formally published context

Terms of Use: Article is made available in accordance with the publisher's policy and may be subject to US copyright law. Please refer to the publisher's site for terms of use.



Preheating after multifield inflation with nonminimal couplings. II. Resonance structure

Matthew P. DeCross,^{1,*} David I. Kaiser,^{1,†} Anirudh Prabhu,^{1,‡} Chanda Prescod-Weinstein,^{2,§} and Evangelos I. Sfakianakis^{3,||}

¹*Department of Physics, Massachusetts Institute of Technology, Cambridge, Massachusetts 02139, USA*

²*Department of Physics, University of Washington, Seattle, Washington 98195-1560, USA*

³*Department of Physics, University of Illinois at Urbana-Champaign, Urbana, Illinois 61801, USA*



(Received 15 November 2016; published 26 January 2018)

This is the second in a series of papers on preheating in inflationary models comprised of multiple scalar fields coupled nonminimally to gravity. In this paper, we work in the rigid-spacetime approximation and consider field trajectories within the single-field attractor, which is a generic feature of these models. We construct the Floquet charts to find regions of parameter space in which particle production is efficient for both the adiabatic and isocurvature modes, and analyze the resonance structure using analytic and semianalytic techniques. Particle production in the adiabatic direction is characterized by the existence of an asymptotic scaling solution at large values of the nonminimal couplings, $\xi_I \gg 1$, in which the dominant instability band arises in the long-wavelength limit, for comoving wave numbers $k \rightarrow 0$. However, the large- ξ_I regime is not reached until $\xi_I \geq \mathcal{O}(100)$. In the intermediate regime, with $\xi_I \sim \mathcal{O}(1-10)$, the resonance structure depends strongly on wave number and couplings. The resonance structure for isocurvature perturbations is distinct and more complicated than its adiabatic counterpart. An intermediate regime, for $\xi_I \sim \mathcal{O}(1-10)$, is again evident. For large values of ξ_I , the Floquet chart consists of densely spaced, nearly parallel instability bands, suggesting a very efficient preheating behavior. The increased efficiency arises from features of the nontrivial field-space manifold in the Einstein frame, which itself arises from the fields' nonminimal couplings in the Jordan frame, and has no analog in models with minimal couplings. Quantitatively, the approach to the large- ξ_I asymptotic solution for isocurvature modes is slower than in the case of the adiabatic modes.

DOI: [10.1103/PhysRevD.97.023527](https://doi.org/10.1103/PhysRevD.97.023527)

I. INTRODUCTION

This paper is the second of a three-part series focusing on the preheating dynamics of multifield models of inflation with nonminimal couplings. (See also Refs. [1,2].) Such models are well motivated: realistic models of high-energy physics generically include many scalar degrees of freedom at high energy scales [3–8], and nonminimal couplings are generically required as renormalization counterterms for interacting scalar fields in curved spacetime [9–15]. The family of models we consider includes well-known examples like Higgs inflation [16] (see also [17–22]), as well as related models with attractorlike solutions [23–27].

The epoch of postinflation reheating is critical for several reasons. (For reviews of reheating, see Refs. [28–33].)

Reheating is responsible for populating the Universe with Standard Model particles in thermal equilibrium. Moreover, understanding the dynamics of reheating is essential for connecting predictions from inflationary models with high-precision measurements of primordial perturbation spectra, since reheating affects the expansion history of the Universe between the end of inflation and eras such as big-bang nucleosynthesis [34–41].

The first stage of reheating is characterized by the resonant decay of the scalar-field condensate(s) that had driven inflation. We use the doubly covariant formalism introduced in Ref. [1], which self-consistently incorporates metric perturbations and field fluctuations to first order and maintains reparametrization freedom of the nontrivial field-space manifold. In this paper we focus on the early stage of preheating, working to linear order in the fluctuations. To simplify, we only consider the decay of the inflaton into nongauged scalar fields, for now ignoring higher-spin particles such as fermions and gauge fields, although we expect that such fields will have a rich phenomenology [32,42–68]. Our study builds upon previous studies of preheating in models with nonminimal couplings and/or noncanonical kinetic terms [69–79], with the aim of identifying characteristic features across a wide range of parameters.

*mdecross@sas.upenn.edu

Now at the Department of Physics and Astronomy, University of Pennsylvania.

†dikaiser@mit.edu

‡anirabhu@stanford.edu

Now at the Department of Physics, Stanford University.

§cprescod@uw.edu

||evans@nikhef.nl

Now at NIKHEF and Leiden University.

In Ref. [1], we identified several distinctions between preheating in multifield models with nonminimal couplings compared to more familiar, minimally coupled models. First, the oscillations of the background fields are affected by the conformal stretching of the fields' potential in the Einstein frame. Second, the single-field attractor behavior tends to enhance efficiency during preheating compared to multifield, minimally coupled models [80,81]. Third, in the limit of strong couplings, $\xi_I \gg 1$, the nontrivial field-space manifold affects the effective masses for adiabatic and isocurvature fluctuations differently, which in turn affects the energy transfer to long-wavelength perturbations. In the present paper we analyze the structure of resonances in this family of models semianalytically and numerically across wide regions of parameter space.

In this paper we adopt the approximation of a rigid spacetime, in which we imagine keeping the energy density fixed while sending $M_{\text{pl}} \rightarrow \infty$. (The reduced Planck mass is given by $M_{\text{pl}} \equiv 1/\sqrt{8\pi G} = 2.43 \times 10^{18}$ GeV.) In that limit, we may neglect the expansion of spacetime during preheating, as well as the effects of the coupled metric perturbations [32]. Then the oscillations of the inflaton condensate(s) become periodic, and we may apply the tools of Floquet theory to study the resonant amplification of perturbations. In Sec. II we examine the background dynamics for a two-field model after inflation, highlighting distinctions between oscillations during preheating with and without nonminimal couplings. We analyze the spectral content of the background oscillations; as shown in Sec. II, analytic progress can be made in the limit of large nonminimal couplings.

Knowledge of the behavior of the background fields during the oscillating phase is critical for understanding the resonant production of particles during preheating. In Sec. III we briefly review the covariant mode expansion for the fluctuations introduced in Ref. [1]. Using this covariant formalism, we may construct Floquet charts and identify the instability bands for the fluctuations. In Sec. IV we analyze the behavior of adiabatic modes and find a universal scaling form for the Floquet chart which emerges in the limit of large nonminimal couplings. In Sec. V the more complex case of isocurvature modes is presented. We construct the three-dimensional Floquet charts for a wide range of nonminimal couplings and potential parameters. In the region of large nonminimal couplings, the Floquet chart is comprised of a dense set of nearly parallel instability bands, indicating a very efficient amplification of isocurvature modes. A scaling solution for large ξ_I is found, similar to the adiabatic case, although the asymptotic limit is reached more slowly for comparable values of ξ_I . Concluding remarks follow in Sec. VI.

II. BACKGROUND DYNAMICS

Following the analysis of Refs. [1,23–26] we study inflationary models with multiple scalar fields coupled

nonminimally to the spacetime Ricci scalar. The formalism developed in those studies may be applied to arbitrary numbers of fields, and in previous work [25] we confirmed that the single-field attractor behavior in these models holds for cases with more than two fields. Nonetheless, in this paper we restrict our attention to models with just two fields, ϕ and χ , which significantly simplifies visualizing various results. We work in $3+1$ spacetime dimensions and choose the mostly plus spacetime metric $(-, +, +, +)$.

We begin with the action in the Jordan frame, in which the fields' nonminimal couplings are explicit:

$$S = \int d^4x \sqrt{-\tilde{g}} \left[f(\phi^I) \tilde{R} - \frac{1}{2} \delta_{IJ} \tilde{g}^{\mu\nu} \partial_\mu \phi^I \partial_\nu \phi^J - \tilde{V}(\phi^I) \right]. \quad (1)$$

We use uppercase Latin letters to label field-space indices, $I, J = 1, 2$. For the remainder of this paper we will consider a two-field model with $\phi^I = \{\phi, \chi\}^T$. Greek letters label spacetime indices, $\mu, \nu = 0, 1, 2, 3$, and tildes denote Jordan-frame quantities. By performing the conformal transformation

$$\tilde{g}_{\mu\nu}(x) \rightarrow g_{\mu\nu} = \frac{2}{M_{\text{pl}}^2} f(\phi^I(x)) \tilde{g}_{\mu\nu}(x), \quad (2)$$

we can bring the gravitational part of the action to the usual Einstein-Hilbert form [82,83]

$$S = \int d^4x \sqrt{-g} \left[\frac{M_{\text{pl}}^2}{2} R - \frac{1}{2} \mathcal{G}_{IJ}(\phi^K) g^{\mu\nu} \partial_\mu \phi^I \partial_\nu \phi^J - V(\phi^I) \right]. \quad (3)$$

The induced field-space metric is given by

$$\mathcal{G}_{IJ}(\phi^K) = \frac{M_{\text{pl}}^2}{2f(\phi^K)} \left[\delta_{IJ} + \frac{3}{f(\phi^K)} f_{,I} f_{,J} \right], \quad (4)$$

where $f_{,I} = \partial f / \partial \phi^I$. Explicit components of $\mathcal{G}_{IJ}(\phi^K)$ for our two-field model may be found in Appendix A of Ref. [1]. We note that models that have canonical kinetic terms in the Jordan frame will nonetheless develop a nontrivial field-space manifold in the Einstein frame [82]. The potential in the Einstein frame is similarly stretched by a conformal factor,

$$V(\phi^I) = \frac{M_{\text{pl}}^4}{4f^2(\phi^I)} \tilde{V}(\phi^I). \quad (5)$$

Renormalization of models with self-coupled scalar fields in curved spacetime requires counterterms of the form $\xi \phi^2 R$ for each nonminimally coupled field [9–15]. We therefore take $f(\phi^I)$ to be of the form

$$f(\phi, \chi) = \frac{1}{2} [M_{\text{pl}}^2 + \xi_\phi \phi^2 + \xi_\chi \chi^2]. \quad (6)$$

Each scalar field ϕ^I couples to the Ricci scalar with its own nonminimal-coupling constant, ξ_I , which we take to be positive.

The form of the potential can be arbitrary. We adopt a simple polynomial potential in the Jordan frame that includes the highest renormalizable interaction terms for scalar fields in $3 + 1$ spacetime dimensions:

$$\tilde{V}(\phi, \chi) = \frac{\lambda_\phi}{4} \phi^4 + \frac{g}{2} \phi^2 \chi^2 + \frac{\lambda_\chi}{4} \chi^4. \quad (7)$$

In order for the potential to be nontachyonic, we must choose $\lambda_I > 0$. Furthermore we neglect bare masses m_I^2 , the effects of which can be studied using the methods developed here and in [1]. On a more practical level, keeping only the quartic potential allows us to compare the resonances and Floquet charts of nonminimally coupled models to their well-studied minimally coupled counterparts [84–86], and identify features that arise due to the nontrivial field-space metric, which is a manifestation of the nonminimal couplings in the Einstein frame.

As discussed in Sec. II B of Ref. [26], observational constraints place restrictions on combinations of couplings at the high-energy scales of inflation. In particular, in models like Higgs inflation [16], one typically finds $\lambda_I \sim \mathcal{O}(10^{-2} - 10^{-4})$ at the energy scales of inflation (the range stemming from uncertainty in the value of the top-quark mass, which affects the running of λ_I under renormalization-group flow) [87–90]. The range of λ_I , in turn, requires $\xi_I \sim \mathcal{O}(10^2 - 10^4)$ at high energies, in order to fit various observational constraints from primordial curvature perturbations—a reasonable range, given that ξ_I typically rises with energy scale under renormalization-group flow, with no UV fixed point [12]. Even with such large values of ξ_I , the inflationary dynamics occur at energy scales well below any nontrivial unitarity cutoff scale. (See Ref. [88] and references therein for further discussion.)

We are interested in the structure of resonances during the preheating phase for this family of models, and hence we consider a broader range of values for the couplings, especially ξ_I . Many features of the resonance structure vary markedly with ξ_I . In particular, we explore three regimes of interest: $0 < \xi_I \leq \mathcal{O}(1)$, $\xi_I \sim \mathcal{O}(1-10)$, and $\xi_I \geq \mathcal{O}(100)$. We also analyze the asymptotic behavior in the strongly coupled limit, $\xi_I \gg 1$.

A. Potential geometry and single-field attractor

Inflation occurs in a regime in which $\xi_I(\phi^I)^2 \gg M_{\text{pl}}^2$ for at least one component, J (for $\xi_I \ll 1$ the condition becomes $\phi^I \gg M_{\text{pl}}$). The potential in the Einstein frame becomes asymptotically flat along each direction of field space, as each field ϕ^I becomes arbitrarily large:

$$V(\phi^I) \rightarrow \frac{M_{\text{pl}}^4 \lambda_I}{4 \xi_I^2} \left[1 + \mathcal{O}\left(\frac{M_{\text{pl}}^2}{\xi_I(\phi^I)^2}\right) \right] \quad (8)$$

(no sum on I). Unless some explicit symmetry constrains all coupling constants in the model to be identical ($\lambda_I = g = \lambda$, $\xi_I = \xi$), then the potential in the Einstein frame will develop ridges and valleys, as shown in Fig. 1. We restrict the parameter space to $-g < \sqrt{\lambda_\phi \lambda_\chi}$, where the potential in both frames (Jordan and Einstein) is positive at all times. Since both the ridges and the valleys satisfy $V > 0$, the Universe will inflate (albeit at different rates) whether the fields evolve along a ridge or a valley toward the global minimum of the potential.

As the right side of Fig. 1 makes clear, multifield models with nonminimal couplings display strong single-field attractor behavior during inflation, across a wide range of couplings and initial conditions [1,25,26]. If the fields happen to begin evolving along the top of a ridge, they will eventually fall into a neighboring valley at a rate that depends on the local curvature of the potential [23,26]. Once the fields fall into a valley, Hubble drag quickly damps out any transverse motions in field space within a few efolds, after which the system evolves with very little turning in field space for the remainder of inflation [23–26].

The orientation of the valley in field space, $\theta = \arctan(\phi/\chi)$, depends on the choice of couplings [23]. As demonstrated in Ref. [1], we may always exploit the covariant framework and perform a rotation in field space, $\phi^I \rightarrow \phi'^I$, such that the valley lies along the direction $\chi' = 0$ during inflation. Once the fields settle into the single-field attractor, the field-space metric becomes effectively diagonal: $\mathcal{G}_{\phi'\chi'} = \mathcal{O}(\chi') \sim 0$.

The fields will only remain near the top of a ridge for a significant duration of inflation if *both* the local curvature of the potential *and* the initial conditions in field-space $\chi(t_0)$ are tuned to be exponentially close to zero. In those cases, the system's evolution during the last 60 efolds of inflation can amplify non-Gaussianities and isocurvature perturbations, which could potentially be observable [23,26,91]. However, if neither the local curvature of the potential nor the fields' initial conditions are exponentially fine-tuned, then the system will rapidly relax into a valley and evolve along an effectively single-field trajectory right to the end of inflation. Within the single-field attractor, these models predict values for spectral observables such as the primordial spectral index and its running (n_s and α), the ratio of power in tensor to scalar modes (r), primordial non-Gaussianity (f_{NL}), and the fraction of power in isocurvature rather than adiabatic scalar modes (β_{iso}) all in excellent agreement with the latest observations [23–26].

We have extensively studied the geometry of the potential and its parameter dependence in Ref. [1]. As discussed there, the single-field attractor behavior in these models

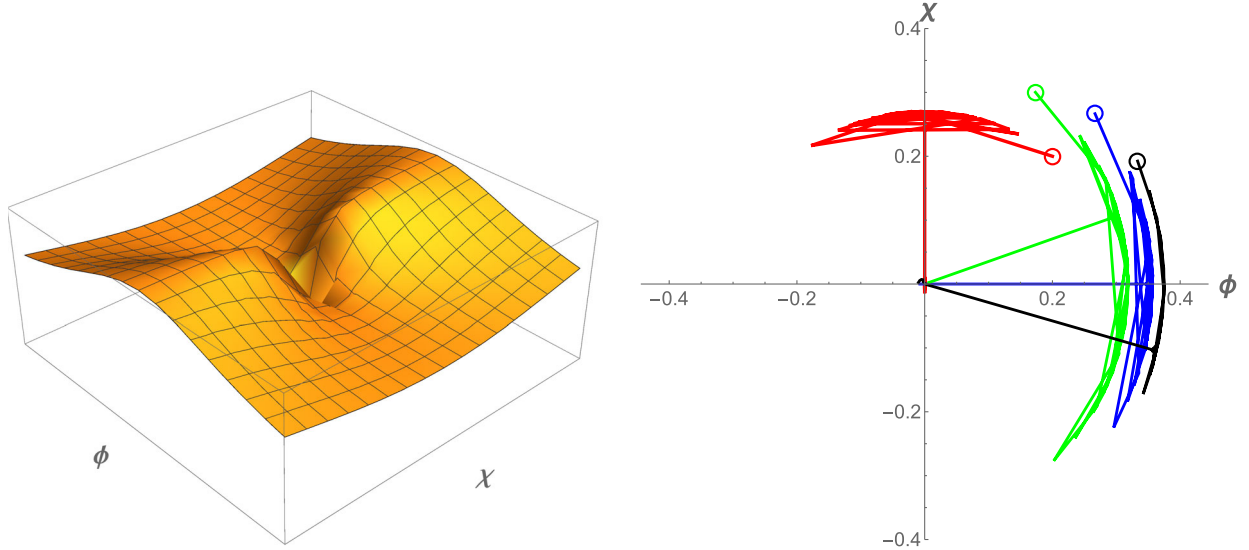


FIG. 1. Left: potential in the Einstein frame, $V(\phi')$, for a two-field model with $\lambda_\chi = 1.25\lambda_\phi$, $g = \lambda_\phi$, and $\xi_\chi = 0.8\xi_\phi$. Right: field trajectories for different couplings and initial conditions (from Ref. [25]). Open circles indicate fields' initial values (in units of M_{pl}). We set the fields' initial velocities to zero and adjust the initial angle in field space, $\theta_0 = \arctan(\phi_0/\chi_0)$. We fix $\lambda_\phi = 10^{-2}$ and $\xi_\phi = 10^3$ and vary the other parameters $\{\lambda_\chi, g, \xi_\chi, \theta_0\}$ as follows: $\{0.75\lambda_\phi, \lambda_\phi, 1.2\xi_\phi, \pi/4\}$ (red), $\{\lambda_\phi, \lambda_\phi, 0.8\xi_\phi, \pi/4\}$ (blue), $\{\lambda_\phi, 0.75\lambda_\phi, 0.8\xi_\phi, \pi/6\}$ (green), and $\{\lambda_\phi, 0.75\lambda_\phi, 0.8\xi_\phi, \pi/3\}$ (black). In each case, the initial transient motion damps out within a few efolds, yielding effectively single-field evolution during inflation.

persists after the end of inflation and into the early phase of preheating, at least to linear order in the fluctuations. For the remainder of this work, we will therefore only consider scenarios in which the background fields evolve within a single-field attractor. Without loss of generality, we consider that attractor to lie along the $\chi = 0$ direction in field space.

B. Spectral content of the oscillating background field

Given the dependence of the effective equation of state on ξ_ϕ while the background field(s) oscillate [1], we expect the oscillations themselves to show significant deviation from the case of minimal couplings. We demonstrated in Ref. [1] that the frequency of oscillation ω exceeds the Hubble expansion rate during preheating in these models, $\omega/H > 1$, across the entire range $10^{-3} \leq \xi_\phi \leq 10^3$ (see Fig. 10 in Ref. [1]). To facilitate comparison with the well-studied case of a minimally coupled field with quartic self-coupling [84–86], we therefore neglect Hubble expansion during the oscillating phase (though its effects may be incorporated perturbatively [92]). We further neglect backreaction from produced particles on the background fields' oscillation. Hence we may employ Fourier analysis to study the dependence of the harmonic structure of the background oscillations on ξ_ϕ .

Although we are working in the rigid-spacetime approximation, we aim to be able to exploit as many results as

possible when considering the more realistic case of an expanding universe in Ref. [2]. Hence it is important to examine the range of background field values that are relevant. Figure 2 shows the behavior of the inflaton background field $\phi(t)$ after the end of inflation, neglecting backreaction. For $\xi_\phi \gtrsim 1$ inflation ends at $\phi \approx 0.8M_{\text{pl}}/\sqrt{\xi_\phi}$ [1]. However, using the rigid-spacetime approximation to study oscillations with amplitude $\phi_{\text{max}} = 0.8M_{\text{pl}}/\sqrt{\xi_\phi}$ introduces a considerable error, since at the end of inflation the Hubble friction term is still non-negligible, leading to a decrease of the inflaton amplitude by a factor of 2 within one oscillation. The most relevant regime for calculating quantities like the period and spectral content of the oscillating inflaton field is therefore $\phi_{\text{max}} = (\alpha \times 0.8)M_{\text{pl}}/\sqrt{\xi_\phi}$ with $0.3 \lesssim \alpha \lesssim 0.5$. These values will capture particle production during the first few oscillations of the inflaton field, for which we may safely neglect backreaction effects. We will restrict our analysis for the remainder of this work to $\phi_{\text{max}} = (0.5 \times 0.8)M_{\text{pl}}/\sqrt{\xi_\phi}$, unless stated otherwise.

Within the single-field attractor, with $H \sim 0$, the background field $\phi(t)$ obeys the equation of motion

$$\ddot{\phi} + \Gamma_{\phi\phi}^{\phi} \dot{\phi}^2 + \mathcal{G}^{\phi\phi} V_{,\phi} \approx 0. \quad (9)$$

We rescale time as $\tau \equiv \sqrt{\lambda_\phi} t$, so that the dynamics depend only on ξ_ϕ . After inflation ends at τ_{end} , $\phi(\tau)$ oscillates with a period given by

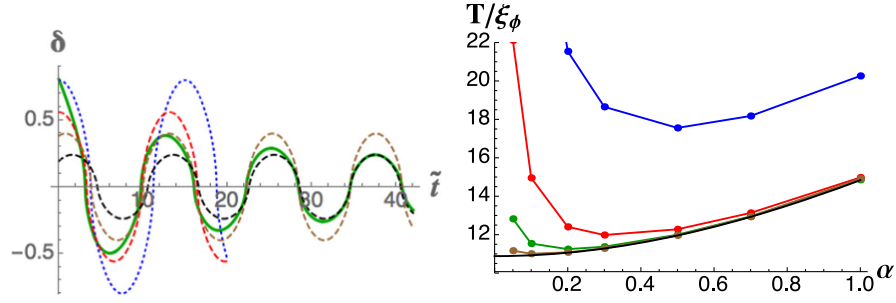


FIG. 2. Left: rescaled background solution $\delta(t) = \sqrt{\xi_\phi} \phi(t)/M_{\text{pl}}$ as a function of $\tilde{t} = \sqrt{\lambda_\phi} M_{\text{pl}} t / \xi_\phi$ after the end of inflation, with $\xi_\phi = 100$. Shown in green is the evolution of $\delta(t)$ when Hubble expansion is included self-consistently. The other curves show the rigid-spacetime solution with initial condition $\delta(0) = (\alpha \times 0.8) \sqrt{\xi_\phi} \phi_0 / M_{\text{pl}}$, with $\alpha = 1, 0.7, 0.5, 0.3$ (blue, red, brown, and black, respectively). Right: rescaled period of background oscillation in a static universe [in units of $(\sqrt{\lambda_\phi} M_{\text{pl}})^{-1}$] for $\xi_\phi = 10, 10^2, 10^3, 10^4$ (top to bottom: blue, red, green, and brown, respectively) as a function of the amplitude parameter α . The analytic approximation for the period in the large- ξ_ϕ regime is shown in black, and is derived under the assumption that $6\xi_\phi \alpha^2 \gg 1$.

$$T = 2 \int_{-\phi_0}^{\phi_0} d\phi \sqrt{\frac{\mathcal{G}_{\phi\phi}}{2V(\phi_0) - 2V(\phi)}}. \quad (10)$$

[We label $\phi_0 = \phi(\tau_{\text{end}})$ as the amplitude of the field at the start of preheating.] The period behaves as $T \propto \xi_\phi$ for $\xi_\phi \gg 1$, as calculated in Appendix B of Ref. [1] and shown in Fig. 2. In the limit $\xi_\phi \gg 1$, the period T rises monotonically with α , though for intermediate values of ξ_ϕ the period shows a more complicated dependence on α .

The terms in Eq. (9) that arise from the nontrivial field-space metric affect the harmonic structure of ϕ 's oscillations. In the limit $\xi_\phi = 0$, with the Jordan-frame potential of Eq. (7), Eq. (9) may be solved analytically as a Jacobian elliptic cosine [84–86]: $\phi(t) = \phi_0 \text{cn}(\phi_0 \tau, 1/\sqrt{2})$. The function $\text{cn}(x, \kappa)$ is periodic with period $4K(\kappa)$, where $K(\kappa)$ is the complete elliptic integral of the first kind [93]. The Jacobian elliptic cosine may be expanded in the infinite series (see Eq. 16.23.2 of [93])

$$\text{cn}(x, \kappa) = \frac{2\pi}{\sqrt{\kappa} K(\kappa)} \sum_{n=0}^{\infty} \frac{q^{n+1/2}}{1 + q^{2n+1}} \cos(4n+2)v, \quad (11)$$

where $q \equiv \exp[-\pi K'/K]$, $v \equiv \pi x/(4K)$, and $K'(\kappa) = K(1 - \kappa)$. Given $\kappa = 1/\sqrt{2}$ for $\xi_\phi = 0$, we find $q = 0.076$, and hence terms with $n \geq 3$ in the series expansion enter with coefficients $\mathcal{O}(10^{-3})$ or less. In the case of minimal coupling, in other words, the oscillations of $\phi(\tau)$ are well approximated by a dominant cosine term and a first harmonic. As shown in Fig. 3, for $\xi_\phi > 0$ the harmonic structure shifts, with (in general) more non-negligible harmonics. This can lead to regions of enhanced resonance during preheating, as we will see in Secs. IV and V.

For arbitrary ξ_ϕ , we may expand $\phi(\tau)$ in a Fourier series. The Fourier coefficients a_n for each harmonic are defined by

$$a_n = \frac{2}{T} \int_0^T d\tau \phi(\tau) \cos\left(\frac{n\pi\tau}{T}\right), \quad (12)$$

with T given by Eq. (10). Given the initial conditions for $\phi(\tau)$ at τ_{end} , the coefficients for all odd n vanish identically. Moreover, as indicated in Eq. (11) for the $\xi_\phi = 0$ case, all a_{4n} for $n \geq 1$ also vanish—a feature that remains true (to within numerical precision) for $\xi_\phi \neq 0$. The only nonzero coefficients of the Fourier expansion are a_{4n+2} for $n \geq 0$.

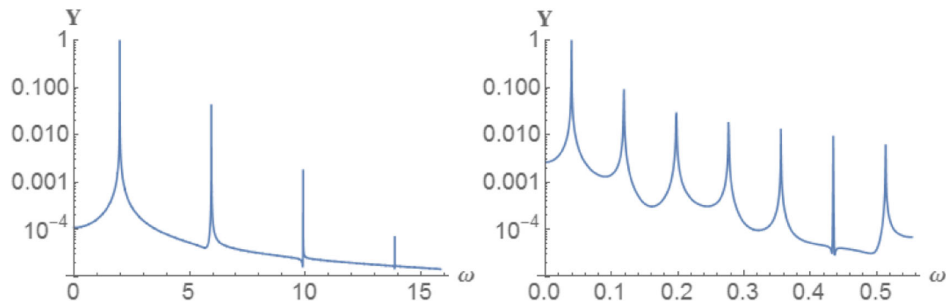


FIG. 3. Fast Fourier transforms of $\phi(\tau)$ for $\xi_\phi = 0$ (left) and $\xi_\phi = 10$ (right). For $\xi_\phi > 0$, the background field's oscillations show a richer spectral content, including more non-negligible harmonics, which may drive additional resonances compared to the $\xi_\phi = 0$ case. All higher harmonics are normalized with respect to the amplitude of the fundamental mode and ω is measured in units of $\sqrt{\lambda_\phi} M_{\text{pl}}$.

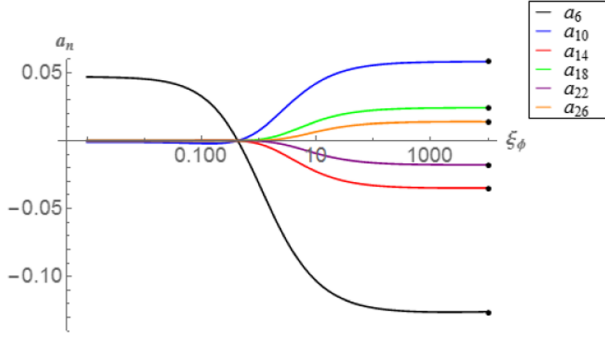


FIG. 4. Magnitudes of the first seven nonzero Fourier coefficients a_n of $\phi(\tau)$ as functions of ξ_ϕ . The a_n have been normalized by the magnitude of the dominant mode a_2 for fixed ξ_ϕ , so a_2 is not displayed. The Fourier coefficients corresponding to the asymptotic solution in the $\xi_\phi \rightarrow \infty$ limit are marked by black dots at the right side of the plot.

In Fig. 4 we plot the first seven nonzero coefficients a_n as functions of ξ_ϕ . Consistent with the behavior in Fig. 3, the first two coefficients dominate in the limit $\xi_\phi \sim 0$, whereas a richer spectrum emerges for $\xi_\phi > 1$. Moreover, the dependence of each a_n on ξ_ϕ becomes nearly flat for $\xi_\phi \geq 100$, indicating a single asymptotic behavior in the limit $\xi_\phi \gg 1$. We can analytically prove the existence of an asymptotic solution for the inflaton oscillation, which is independent of ξ_ϕ in the limit of $\xi_\phi \rightarrow \infty$, if we rescale the field as $\delta \equiv \sqrt{\xi_\phi} \phi / M_{\text{pl}}$ and time as $\tilde{t} \equiv M_{\text{pl}} \tau / \xi_\phi = \sqrt{\lambda_\phi} M_{\text{pl}} t / \xi_\phi$. Performing these operations we arrive at the ξ_ϕ -independent asymptotic equation of motion

$$\ddot{\delta} + \frac{1 - \delta^2}{\delta(1 + \delta^2)} \dot{\delta}^2 + \frac{1}{6} \frac{\delta}{1 + \delta^2} = 0. \quad (13)$$

Details of the derivation and solution of Eq. (13) are given in Appendix A.

In the limit $\xi_\phi \rightarrow \infty$, for which the background solutions $\delta(t)$ satisfy Eq. (13), we find the Fourier coefficients (a_2, a_6, a_{10}, \dots) to be

$$\{a_{4n+2}\} \approx \{1, -0.1265, 0.05813, -0.03513, 0.02415, -0.01790, 0.01396, \dots\}, \quad (14)$$

where we have normalized the amplitude of the dominant mode to unity. We note both an alternation between positive and negative values for rising n , as well as a falling magnitude. As can be seen in Fig. 4, the Fourier coefficients calculated numerically for finite ξ_ϕ quickly asymptote to these values once the nonminimal coupling reaches $\xi_\phi \approx 100$. On the other hand, there remains significant variation of the Fourier coefficients a_n with ξ_ϕ for $\xi_\phi \sim \mathcal{O}(10)$. Whereas the inflationary observables, such as the spectral index n_s and the tensor-to-scalar ratio r ,

attain their large- ξ_ϕ values by $\xi_\phi \approx 10$ [23–26], the post-inflationary dynamics are sensitive to three distinct regimes for ξ_ϕ , with behavior for $0 < \xi_\phi < 1$ distinct from $\xi_\phi \sim \mathcal{O}(1-10)$, which in turn remains distinct from the regime with $\xi_\phi \geq 100$. For preheating, in other words, there exists an intermediate- ξ_ϕ regime, with important consequences for particle production.

For $\xi_\phi > 0$, another significant modification to the oscillation of $\phi(\tau)$ may occur, compared to the $\xi_\phi = 0$ case. In the equation of motion for ϕ , Eq. (9), the two distinct contributions from the nontrivial field-space metric—the noncanonical kinetic term and the conformal stretching of the Einstein-frame potential—may exactly cancel, resulting in *simpler* motion for $\phi(\tau)$ than in the minimally coupled case. In particular, for a specific amplitude $\phi_0 = \tilde{\phi}_0(\xi_\phi)$, with

$$\tilde{\phi}_0 \equiv \frac{M_{\text{pl}}}{\sqrt{\xi_\phi(6\xi_\phi - 1)}} \quad (15)$$

and $\xi_\phi > 1/6$, Eq. (9) reduces to $\phi'' + m^2 \phi = 0$, where primes denote $d/d\tau$ and

$$m^2 = \frac{(6\xi_\phi - 1)}{72\xi_\phi^3} M_{\text{pl}}^2. \quad (16)$$

In that case the background field motion is sinusoidal, $\phi(\tau) = \tilde{\phi}_0 \cos(m\tau)$, with period

$$T = \frac{2\pi}{m} = \frac{12\pi}{M_{\text{pl}}} \sqrt{\frac{2\xi_\phi^3}{6\xi_\phi - 1}}, \quad (17)$$

in exact agreement with the value of T calculated from Eq. (10). We thereby find that the inherently anharmonic oscillations in the $\xi_\phi = 0$ case, arising from the nonlinear equation of motion $\phi'' + \phi^3 = 0$, may reduce for $\xi_\phi > 1/6$ to purely harmonic motion for a special value of the amplitude. The fact that there is dependence on the amplitude is not surprising, given that Eq. (9) is a highly nonlinear equation.

Given an initial amplitude of oscillation ϕ_0 at τ_{end} determined self-consistently from the criterion $\epsilon \equiv -\dot{H}/H^2 = 1$, we may invert the relation between $\tilde{\phi}_0$ and ξ_ϕ in Eq. (15) to find the value of ξ_ϕ at which all higher harmonics vanish. In Fig. 5 we plot the Fourier coefficients a_{4n+2} for $n \geq 1$ in the regime $0 \leq \xi_\phi \leq 1$, and find that all higher harmonics vanish at $\xi_\phi \approx 0.486$. We note, however, that $\tilde{\phi}_0 \sim \xi_\phi^{-1}$ in the limit of large ξ_ϕ , whereas the amplitude of the inflaton at the end of inflation scales as $\phi_0 \sim \xi_\phi^{-1/2}$, so that the special, simple oscillation of $\phi(t)$ is unlikely to be relevant in the limit $\xi_\phi \gg 1$ before nonlinear effects such as backreaction alter the dynamics.

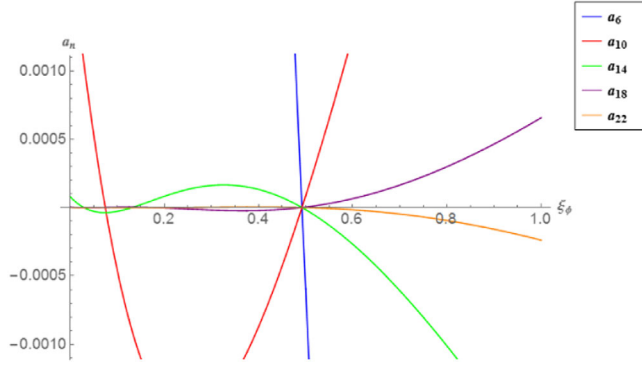


FIG. 5. The behavior of the Fourier coefficients a_{n+2} for $n \geq 1$ within the range $0 \leq \xi_\phi \leq 1$. For a given initial amplitude, ϕ_0 , there exists a single value ξ_ϕ at which all higher harmonics vanish identically, leaving purely harmonic evolution for $\phi(\tau)$.

In summary, we find that the oscillations of $\phi(\tau)$ display richer harmonic structure for $\xi_\phi > 0$ than for the $\xi_\phi = 0$ case. For most values of ξ_ϕ , we find more non-negligible harmonics than for the minimally coupled case, and the magnitudes of those harmonics rapidly asymptote to fixed values for $\xi_\phi \geq 100$. Meanwhile, for a special amplitude of oscillation, all higher harmonics vanish, again in distinction to the $\xi_\phi = 0$ case. We now turn to the fluctuations, which can be parametrically amplified by the periodic motion of the background field.

III. EVOLUTION OF THE FLUCTUATIONS

In Ref. [1] we established a framework with which to study the evolution of the gauge-invariant fluctuations Q^I during preheating, by expanding the action to second order in both field and metric perturbations, calculating the energy density, and performing a (covariant) mode expansion. This framework will enable us to use Floquet analysis to examine how the resonance structure changes in the presence of $\xi_I \neq 0$ compared to the minimally coupled case.

To first order in the fluctuations, the equation of motion for Q^I may be written [1]

$$\mathcal{D}_t^2 Q^I + 3H\mathcal{D}_t Q^I + \left[\frac{k^2}{a^2} \delta_J^I + \mathcal{M}_J^I \right] Q^J = 0. \quad (18)$$

Here $\mathcal{D}_J Q^I = \partial_J Q^I + \Gamma^I_{JK} Q^K$ is the covariant derivative with respect to the field-space metric \mathcal{G}_{IJ} , in terms of which the directional derivative may be written $\mathcal{D}_I Q^I = \dot{\varphi}^I \mathcal{D}_I Q^I$, where $\varphi^I(t)$ are the spatially homogenous background fields. The mass-squared matrix is given by

$$\begin{aligned} \mathcal{M}_J^I &= \mathcal{G}^{IK} (\mathcal{D}_J \mathcal{D}_K V) - \mathcal{R}^I_{LMJ} \dot{\varphi}^L \dot{\varphi}^M \\ &\quad - \frac{1}{M_{\text{pl}}^2 a^3} \mathcal{D}_I \left(\frac{a^3}{H} \dot{\varphi}^I \dot{\varphi}_J \right), \end{aligned} \quad (19)$$

where \mathcal{R}_{ILMJ} is the Riemann tensor constructed from \mathcal{G}_{IJ} , and the last term in Eq. (19) arises from the coupled metric perturbations.

We follow the decomposition of the perturbations using field-space vielbeins, as discussed in detail in Sec. IV A of Ref. [1]. We rescale the fluctuations, $Q^I(x^\mu) \rightarrow X^I(x^\mu)/a(t)$, and quantize, $X^I \rightarrow \hat{X}^I$, expanding the fluctuations in creation and annihilation operators and associated mode functions:

$$\begin{aligned} \hat{X}^\phi(x^\mu) &= \int \frac{d^3 k}{(2\pi)^{3/2}} [(v_k e_1^\phi \hat{b}_{\mathbf{k}} + w_k e_2^\phi \hat{c}_{\mathbf{k}}) e^{i\mathbf{k} \cdot \mathbf{x}} \\ &\quad + (v_k^* e_1^\phi \hat{b}_{\mathbf{k}}^\dagger + w_k^* e_2^\phi \hat{c}_{\mathbf{k}}^\dagger) e^{-i\mathbf{k} \cdot \mathbf{x}}], \\ \hat{X}^\chi(x^\mu) &= \int \frac{d^3 k}{(2\pi)^{3/2}} [(y_k e_1^\chi \hat{b}_{\mathbf{k}} + z_k e_2^\chi \hat{c}_{\mathbf{k}}) e^{i\mathbf{k} \cdot \mathbf{x}} \\ &\quad + (y_k^* e_1^\chi \hat{b}_{\mathbf{k}}^\dagger + z_k^* e_2^\chi \hat{c}_{\mathbf{k}}^\dagger) e^{-i\mathbf{k} \cdot \mathbf{x}}], \end{aligned} \quad (20)$$

where the operators obey $\hat{b}_{\mathbf{k}}|0\rangle = \hat{c}_{\mathbf{k}}|0\rangle = 0$ for all \mathbf{k} , and

$$\begin{aligned} [\hat{b}_{\mathbf{k}}, \hat{b}_{\mathbf{q}}^\dagger] &= [\hat{c}_{\mathbf{k}}, \hat{c}_{\mathbf{q}}^\dagger] = \delta^{(3)}(\mathbf{k} - \mathbf{q}), \\ [\hat{b}_{\mathbf{k}}, \hat{c}_{\mathbf{q}}] &= [\hat{b}_{\mathbf{k}}, \hat{c}_{\mathbf{q}}^\dagger] = 0. \end{aligned} \quad (21)$$

Within the single-field attractor, $\mathcal{G}_{\phi\chi} \sim 0$ and hence $e_1^\chi \sim e_2^\phi \sim 0$, so that the equations of motion for the mode functions effectively decouple:

$$\begin{aligned} v_k'' + \Omega_{(\phi)}^2(k, \eta) v_k &\simeq 0, \\ z_k'' + \Omega_{(\chi)}^2(k, \eta) z_k &\simeq 0, \end{aligned} \quad (22)$$

where here primes denote derivatives with respect to conformal time, $d\eta \equiv dt/a(t)$, and the effective frequencies are given by

$$\begin{aligned} \Omega_{(\phi)}^2(k, \eta) &= k^2 + a^2 m_{\text{eff},\phi}^2(\eta), \\ \Omega_{(\chi)}^2(k, \eta) &= k^2 + a^2 m_{\text{eff},\chi}^2(\eta). \end{aligned} \quad (23)$$

The effective masses may be decomposed into four distinct contributions [1],

$$m_{\text{eff},\phi}^2 = m_{1,\phi}^2 + m_{2,\phi}^2 + m_{3,\phi}^2 + m_{4,\phi}^2, \quad (24)$$

with

$$\begin{aligned} m_{1,\phi}^2 &\equiv \mathcal{G}^{\phi K} (\mathcal{D}_\phi \mathcal{D}_K V), \\ m_{2,\phi}^2 &\equiv -\mathcal{R}_{LM\phi}^\phi \dot{\varphi}^L \dot{\varphi}^M, \\ m_{3,\phi}^2 &\equiv -\frac{1}{M_{\text{pl}}^2 a^3} \delta_1^\phi \delta_2^\phi \mathcal{D}_I \left(\frac{a^3}{H} \dot{\varphi}^I \dot{\varphi}_J \right), \\ m_{4,\phi}^2 &\equiv -\frac{1}{6} R, \end{aligned} \quad (25)$$

where R is the spacetime Ricci curvature scalar; comparable expressions follow for the contributions to $m_{\text{eff},\chi}^2$.

Within the rigid-spacetime approximation, $a(t) \rightarrow 1$, $\eta \rightarrow t$, and $m_{3,I}^2, m_{4,I}^2 \rightarrow 0$. Then the only contributions to the fluctuations' effective masses arise from the (covariant) curvature of the potential ($m_{1,I}^2$) and from the curved field-space manifold ($m_{2,I}^2$). (As indicated in Refs. [1,71,94–102] and further analyzed in Ref. [2], the contributions from the metric perturbations, $m_{3,I}^2$, may become significant in certain regions of parameter space when one relaxes the rigid-spacetime approximation.)

Since we are considering motion of the background fields within a single-field attractor along the direction $\chi = 0$, $v_k \sim \delta\phi_k$ corresponds to fluctuations in the adiabatic direction, and $z_k \sim \delta\chi_k$ corresponds to fluctuations in the isocurvature direction. The corresponding energy densities are given by [1]

$$\rho_k^{(\phi)} = \frac{1}{2} (|\dot{v}_k|^2 + \Omega_{(\phi)}^2(k, t) |v_k|^2), \quad (26)$$

$$\rho_k^{(\chi)} = \frac{1}{2} (|\dot{z}_k|^2 + \Omega_{(\chi)}^2(k, t) |z_k|^2). \quad (27)$$

We measure particle production with respect to the instantaneous adiabatic vacuum, $|0(t_{\text{end}})\rangle$, which minimizes the energy densities $\rho_k^{(I)}$ at the end of inflation [32].

Within the rigid-spacetime approximation, the frequencies $\Omega_{(I)}^2(k, t)$ oscillate periodically as the background field $\phi(t)$ oscillates periodically. Floquet's theorem then stipulates that solutions to Eq. (22) may be written in the form $v_k(t) = P_1(k, t) \exp[\mu_k t] + P_2(k, t) \exp[-\mu_k t]$ for some periodic functions $P_{1,2}$, and likewise for $z_k(t)$ [32]. The Floquet exponents μ_k depend, in general, on the couplings, the background oscillation amplitude ϕ_{max} , and the wave number k . Regions of parameter space for which $\text{Re}[\mu_k] \neq 0$ correspond to exponential instabilities, within which the energy densities $\rho_k^{(I)}$ grow rapidly due to particle production.

In the next two sections, we follow the method of Sec. 3.2 of Ref. [32] to construct Floquet charts showing regions with $\text{Re}[\mu_k] \neq 0$ for both adiabatic and isocurvature fluctuations. Whereas calculating the full Floquet chart for this system is a numerical task, semianalytic progress can be made if one wishes to calculate the boundaries of the instability bands, where the real parts of the Floquet exponents vanish. Since the boundaries of the bands are defined by $\text{Re}[\mu_k] = 0$, the resulting perturbations $v_k(t)$ and $z_k(t)$ will be periodic there, with period simply related to the periods of the functions $\Omega_{(\phi)}^2(k, t)$ and $\Omega_{(\chi)}^2(k, t)$.

Assuming a rigid spacetime, the only time dependence for the frequencies $\Omega_{(I)}^2(k, t)$ comes from $m_{1,I}^2(t)$ and $m_{2,I}^2(t)$, which themselves depend on $\phi(t)$ and $\dot{\phi}(t)$. The

periods T_n of $[\phi(t)]^n$ and $[\dot{\phi}(t)]^n$ are given by T if n is odd and $T/2$ if n is even, where T is the period of $\phi(t)$. This fact enormously simplifies our consideration of the periods of complicated functions, since in the nonvanishing components of \mathcal{M}_I^I , the only terms that arise are constants and terms of the form $\phi^{2n}(t)$ and $\dot{\phi}^{2n}(t)$, which are all $T/2$ periodic. It follows that each of the relevant components is $T/2$ -periodic. Therefore, the period of both $\Omega_{(\phi)}^2$ and $\Omega_{(\chi)}^2$ is half that of the background-field oscillation. We thus look for regions in $(g/\lambda_\phi, k^2)$ space that give solutions to Eq. (22) that are either $T/2$ or T periodic, since these give the boundaries of stability bands. The details of the method are presented in Appendix B and the results are shown in Sec. V, where they are compared with full numerical calculations of the Floquet charts.

We further note that the exponents μ_k have units of inverse time, meaning that the magnitude of μ_k should be defined in comparison to some time scale. For preheating the relevant time scale is the Hubble time at the end of inflation. The Hubble time scales like $1/\xi_\phi$ for large ξ_ϕ [1]; hence one relevant parameter that we could plot and compare is $\mu_k \xi_\phi$. This is still a dimensionful quantity, but it has the same parameter dependence as the dimensionless combination μ_k/H . However, one might object to using the Hubble scale as a measure of time in the rigid-spacetime approximation. Instead one may compare the rate μ_k to the period of background oscillations T , and use the quantity $\mu_k T$. For $\xi_\phi \gg 1$ we found above that $T \sim \xi_\phi$; hence both normalization schemes scale in the same way with ξ_ϕ : $\mu_k T \sim \mu_k/H \sim \mu_k \xi_\phi$ in the limit $\xi_\phi \gg 1$. [Recall from Sec. II that the period T is measured in units of $(\sqrt{\lambda_\phi} M_{\text{pl}})^{-1}$.]

Similarly, k is a dimensionful quantity, so we again need to divide by some energy scale in order to find meaningful results. The only energy scale in the problem is the Hubble energy, so the relevant combination is again $k \xi_\phi$. In a static universe, we may consider a characteristic length scale l , defined as $l = cT$, which again gives the same relevant scaling for large ξ_ϕ : $kT \sim k \xi_\phi$ for $\xi_\phi \gg 1$. Since in the limit of large ξ_ϕ , the scaling with T and H are equivalent, we will scale the Floquet exponents and wave numbers by the period of the background oscillation (or simply by ξ_ϕ) for the remainder of this paper.

It is worth reiterating the applicability and limitation of the Floquet formalism, which requires adopting the rigid-spacetime approximation. For example, one may be concerned about whether such an analysis can accurately describe how long-wavelength modes, with $k \ll aH$, would behave in an expanding universe, since such modes should be sensitive to the expansion of spacetime. However, as shown in Ref. [42], even the behavior of the $k = 0$ mode and its transition from the broad- to the narrow-resonance regime in an expanding universe may be understood from an analysis of the corresponding

(rigid-spacetime) Floquet charts. More generally, modes whose Floquet exponent (as calculated within the rigid-spacetime approximation) satisfies $\text{Re}[\mu_k] \gg H$ will be significantly amplified in an expanding universe. One may estimate the resulting amplification by considering how a given mode would “flow” through the instability bands of a Floquet chart, as both the mode’s physical wave number and the amplitude of the oscillating background field redshift. (See, e.g., Refs. [32,33,42,60,66,67].) Thus Floquet analysis can often yield both a general intuition as well as a quantitative guide to how the system would behave in a dynamical spacetime, at least for linearized dynamics (before fully nonlinear interactions dominate).

We may now explore the growth rate of perturbations for various values of the nonminimal couplings, potential parameters, and wave numbers. Since scanning the parameter space by brute force is rather impractical (and would not provide much physical insight), we divide our analysis into subsections, each focusing on a specific range of parameters and type of perturbation (adiabatic or isocurvature). We focus on background-field trajectories within a single-field attractor, and consider (without loss of generality) the attractor to lie along the direction $\chi = 0$. As demonstrated in Ref. [1], we may always exploit our covariant framework and perform a rotation in field space so that the attractor lies along the $\chi = 0$ direction.

IV. RESULTS: ADIABATIC MODES

We begin the analysis with the adiabatic modes, which are simpler than the isocurvature modes since their behavior depends only on ξ_ϕ and k . Within the single-field attractor, the contribution to $m_{\text{eff},\phi}^2$ arising from the curved field-space manifold vanishes, $m_{2,\phi}^2 \sim \mathcal{O}(\chi\dot{\chi}) \sim 0$ [1]. In the rigid-spacetime approximation, therefore, the only contribution to $m_{\text{eff},\phi}^2$ comes from gradients of the potential, $m_{1,\phi}^2$, and may be written

$$m_{\text{eff},\phi}^2 = \frac{-2\delta^6(6\xi_\phi + 1) + \delta^4(12\xi_\phi + 1) + 3\delta^2}{(\delta^2 + 1)^2 \xi_\phi (\delta^2(6\xi_\phi + 1) + 1)^2} M_{\text{pl}}^2, \quad (28)$$

where again $\tau = \sqrt{\lambda_\phi} t$ and $\delta(\tau) = \sqrt{\xi_\phi} \phi(\tau)/M_{\text{pl}}$ is the rescaled field amplitude. In the limit $\xi_\phi \gg 1$ we may further simplify the effective mass:

$$m_{\text{eff},\phi}^2 \approx \frac{M_{\text{pl}}^2}{\xi_\phi^2} \frac{(1 - \delta^2)}{3(1 + \delta^2)^2}, \quad (29)$$

where we have set $1 + \xi_\phi \approx \xi_\phi$ as well as $1 + \xi_\phi \delta^n \approx \xi_\phi \delta^n$, since the regime of interest corresponds to $\delta \sim \mathcal{O}(1)$. [Obviously the second of these approximations fails whenever $\delta(t)$ passes through zero.] If we again rescale time by ξ_ϕ as $\tilde{t} \equiv M_{\text{pl}} \tau / \xi_\phi = \sqrt{\lambda_\phi} M_{\text{pl}} t / \xi_\phi$, the equation of motion for the adiabatic modes in Eq. (22) takes the form

$$\ddot{v}_k + (\tilde{k}^2 + \tilde{m}_{\text{eff},\phi}^2) v_k = 0, \quad (30)$$

where $\tilde{k} = \xi_\phi k / (\sqrt{\lambda_\phi} M_{\text{pl}})$, $\tilde{m}_{\text{eff},\phi}^2 = \xi_\phi^2 m_{\text{eff},\phi}^2 / M_{\text{pl}}^2$, and overdots denote $d/d\tilde{t}$. As shown in Fig. 6 (and also highlighted in Ref. [79]), not only does $\tilde{m}_{\text{eff},\phi}^2(\tilde{t})$ oscillate as $\phi(\tilde{t})$ oscillates but it also develops sharp features, which become more pronounced for $\xi_\phi \gg 1$, asymptoting to a single, self-similar behavior in the limit $\xi_\phi \rightarrow \infty$.

As expected, the time dependence of $\tilde{m}_{\text{eff},\phi}^2(\tilde{t})$ drives parametric resonances in the adiabatic modes $v_k(\tilde{t})$. Figure 7 summarizes the dependence of the (real part of the) Floquet exponent on the wave number and the non-minimal coupling. Starting with the large- ξ_ϕ regime, where interesting self-similar behavior can be found, we see that the Floquet chart for $\xi_\phi \gg 1$ asymptotes to a common shape, once μ_k and k are rescaled by ξ_ϕ , as explained in Sec. III. The large- ξ_ϕ scaling behavior may be understood analytically: after rescaling time and wave number by ξ_ϕ in Eq. (30), ξ_ϕ drops out of the equation altogether.

In the small- ξ_ϕ regime, the dominant Floquet band occurs at a nonzero wave number. As ξ_ϕ increases from 0 to 1, the band moves to larger wave numbers and the magnitude of $\text{Re}[\mu_k]T$ is enhanced by as much as 30%. For $\xi_\phi \sim 1$, a new band emerges at $k \sim 0$. As ξ_ϕ increases further and we move into the large- ξ_ϕ regime, the band at $k \sim 0$ becomes the dominant band. For asymptotically large ξ_ϕ , the value of $\text{Re}[\mu_k]T$ for the dominant band at $k \sim 0$ becomes about 6 times larger than for the secondary instability band.

In Fig. 8 we plot $\rho_k^{(\phi)}$ for various values of ξ_ϕ and for the wave number $\tilde{k}^2 = 0.03$. Consistent with the scaling of the Floquet exponents shown in Fig. 7, we find three distinct regimes for ξ_ϕ at these long wavelengths: no growth for $\xi_\phi = 1$, modest growth for $\xi_\phi = 10$, and then a quick

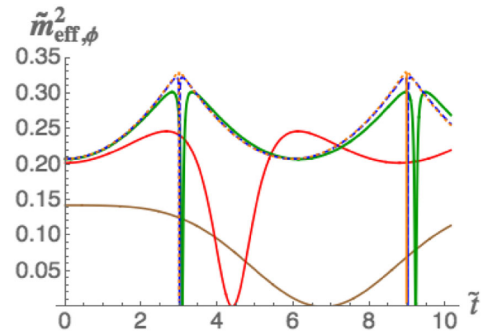


FIG. 6. Rescaled effective mass for the adiabatic perturbations, $\tilde{m}_{\text{eff},\phi}^2 = \xi_\phi^2 m_{\text{eff},\phi}^2$ (in units of M_{pl}^2) versus $\tilde{t} \equiv \sqrt{\lambda_\phi} M_{\text{pl}} t / \xi_\phi$, for $\xi_\phi = 1, 10, 10^2, 10^3, 10^4$ (brown, red, green, blue, and orange, respectively), with $m_{\text{eff},\phi}^2$ given in Eq. (28). The sharp features become more pronounced in the limit $\xi_\phi \gg 1$, and asymptote to a single, self-similar behavior.

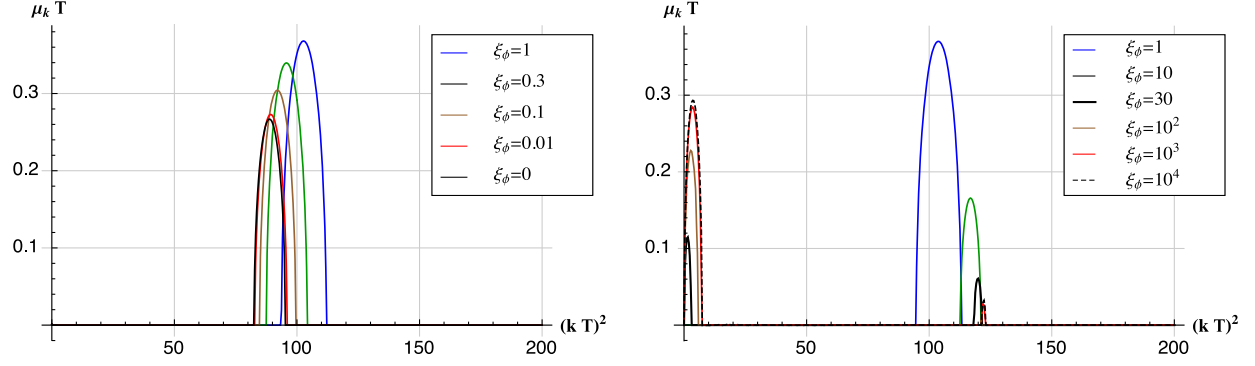


FIG. 7. Left: normalized Floquet exponent $\text{Re}[\mu_k]T$ for the adiabatic mode v_k for $0 \leq \xi_\phi \leq 1$. Right: normalized Floquet exponent $\text{Re}[\mu_k]T$ for the adiabatic mode v_k for $\xi_\phi \geq 1$. The common behavior for $\xi_\phi \gg 1$ is evident.

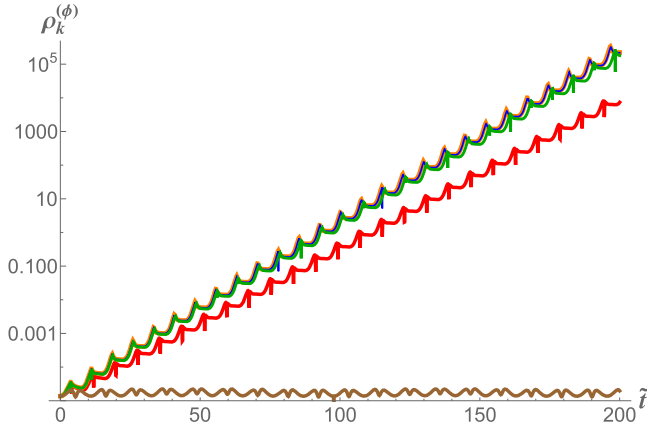


FIG. 8. Energy density $\rho_k^{(\phi)}$ versus $\tilde{t} = \sqrt{\lambda_\phi} M_{\text{pl}} t / \xi_\phi$ for $\tilde{k}^2 = [\xi_\phi k / (\sqrt{\lambda_\phi} M_{\text{pl}})]^2 = 0.03$ and $\xi_\phi = 1, 10, 10^2, 10^3, 10^4$ (bottom to top: brown, red, green, blue, and orange, respectively). The energy density rapidly asymptotes to a single behavior in the limit of large ξ_ϕ .

approach to a single behavior of rapid growth for $\xi_\phi \geq 10^2$. (Because we are neglecting nonlinear effects like the backreaction of created particles on the evolution of the background field, the exponential growth of $\rho_k^{(\phi)}$ within a given resonance band appears to continue forever. Of course when nonlinear effects are incorporated, the resonant amplification will end after a characteristic time [32,67,68,96], though such effects are beyond the scope of the present study.)

In Fig. 9, we zoom in on modes $\tilde{k} \ll 1$, which lie within the dominant Floquet instability band in the limit $\xi_\phi \gg 1$. On the right-hand side we plot the energy density of the adiabatic modes. The black-dotted lines correspond to exact exponential growth at the corresponding value of the Floquet exponent, $\exp(2\text{Re}[\mu_k]t)$; they match very well with the late-time exponential growth of $\rho_k^{(\phi)}$ at various wave numbers. The behavior of the $k = 0$ mode seems quite paradoxical at first. According to the Floquet chart,

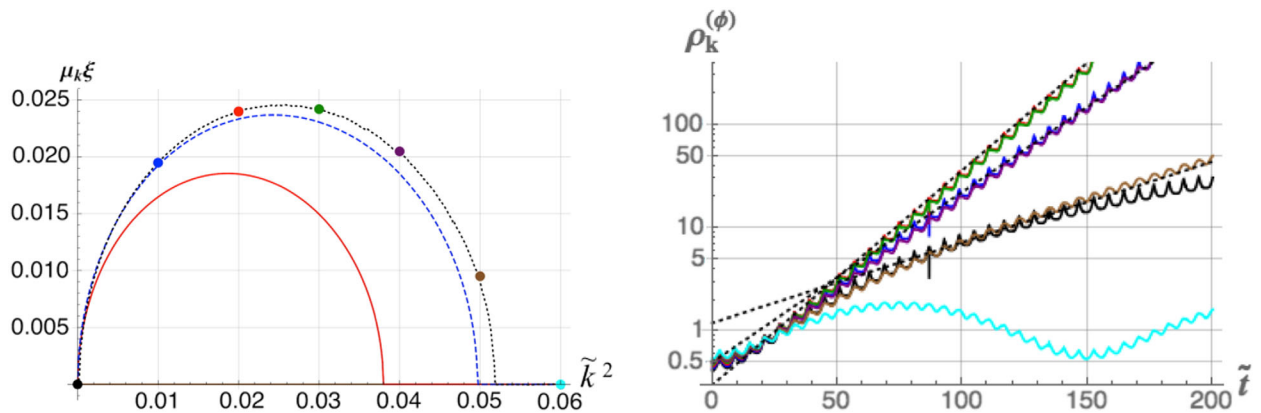


FIG. 9. Left: Floquet chart for adiabatic perturbations with $\xi_\phi = 10^2, 10^3, 10^4$ (red, blue, and black, respectively). The colored dots correspond to the rescaled wave numbers $\tilde{k} = \xi_\phi k / (\sqrt{\lambda_\phi} M_{\text{pl}})$ used in the right panel. Right: energy density for the adiabatic mode with $\xi_\phi = 10^4$ and $\tilde{k}^2 = 0, 0.01, 0.02, 0.03, 0.04, 0.05, 0.06$ (black, blue, red, green, purple, brown, and cyan, respectively). The black-dotted lines correspond to exact exponential growth, $\exp(2\text{Re}[\mu_k]t)$. Note that the Floquet chart (left) is normalized with respect to ξ_ϕ , to make the comparison with the evolution of the energy density as a function of $\tilde{t} = \sqrt{\lambda_\phi} M_{\text{pl}} t / \xi_\phi$ (right) easier.

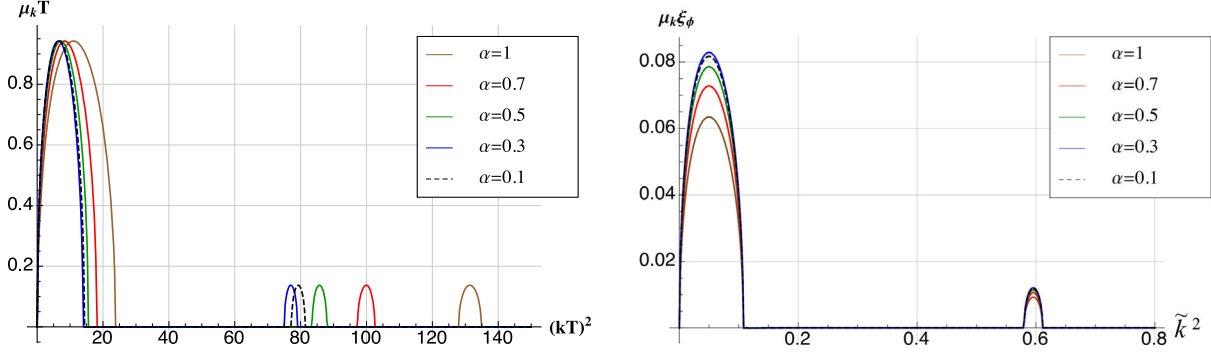


FIG. 10. The Floquet chart for adiabatic perturbations with $\xi_\phi = 10^3$, and the amplitude of the background oscillation parametrized as $\delta(0) = (\alpha \times 0.8) \sqrt{\xi_\phi} \phi_0 / M_{\text{pl}}$, with varying α . Left: Floquet exponent versus wave number, each scaled by the period of background oscillations T . Right: Floquet exponent scaled by the nonminimal coupling ξ_ϕ , versus the rescaled wave number $\tilde{k} = \xi_\phi k / (\sqrt{\lambda_\phi} M_{\text{pl}})$.

$\text{Re}[\mu_{k=0}] = 0$. We would therefore expect the mode to be nongrowing, or at most oscillating like the $\tilde{k}^2 = 0.06$ mode. However we see that the growth is not exponential, but rather polynomial, with $v_k(\tilde{t}) \propto \tilde{t}$, which is the growth exhibited by systems having two zero eigenvalues. Hence the growth of the $k = 0$ mode is consistent with the Floquet chart.

Next we consider the effect of the background amplitude parameter α on the amplification of adiabatic modes. The Floquet chart for large ξ_ϕ and varying values of α is shown in Fig. 10. An interesting phenomenon occurs depending on the choice of normalization. If one normalizes the Floquet exponent and wave number by T , then each band has a constant amplitude for different values of α , but differs in width and position. However, if one normalizes by ξ_ϕ , then each band has a fixed position and width, but its amplitude varies as a function of α . Using ξ_ϕ as a normalization parameter is physically justified if we use the appropriate factors of M_{pl} to construct a dimensionless quantity.

In sum, we identified a scaling solution for the growth of adiabatic modes at large ξ_ϕ . The Floquet chart accurately predicts the late-time growth rate of the adiabatic modes. As one increases ξ_ϕ , the Floquet chart approaches an asymptotic form. The most important difference between the large- ξ_ϕ resonance structure and the corresponding structure for the minimally coupled case is the emergence of a dominant instability band around $k \sim 0$ for large nonminimal coupling. The fact that the dominant band corresponds to $k \sim 0$ means that overall amplification should be increased, compared to the minimally coupled case: physical modes in an expanding universe will redshift toward the resonance band rather than out of it. In the meantime, special care is required for handling the $k = 0$ mode, which grows linearly in a static universe.

V. RESULTS: ISOCURVATURE MODES

We now proceed to the case of isocurvature perturbations, where the dependence of μ_k on g/λ_ϕ and ξ_ϕ/ξ_χ

provides room for richer phenomenology. Since we want to satisfy the attractor condition along the $\chi = 0$ direction, we will choose $g/\lambda_\phi \geq 1$, which, as shown in Sec. III A of Ref. [1], is a sufficient condition for a potential valley along that direction for $\xi_\phi = \xi_\chi$ and any nonzero value of ξ_ϕ .

We start with $\xi_\phi \leq 1$. As shown in Fig. 11, the results for $\xi_\phi = 0$ reproduce the familiar Lamé chart for the minimally coupled case [84–86]. As we increase ξ_ϕ , the bands get shifted to lower values of the coupling g/λ_ϕ , and tilted further away from the g/λ_ϕ axis. The regions with $\text{Re}[\mu_k] \neq 0$ become reduced in width and height. In other words, in the regime $0 < \xi_\phi \leq 1$, preheating is less efficient than in the minimally coupled case.

This situation is reversed in the large- ξ_ϕ regime. In order to study this regime we perform one further rescaling, by the dimensionless quantity g/λ_ϕ . As discussed in Ref. [1], for large ξ_ϕ the direction $\chi = 0$ will be an attractor in field space whenever $\tilde{\Lambda}_\phi < 0$, where

$$\tilde{\Lambda}_\phi \equiv \frac{\xi_\chi}{\xi_\phi} - \frac{g}{\lambda_\phi}. \quad (31)$$

The strength of the attractor is governed by the combination $\tilde{\Lambda}_\phi \xi_\phi$; hence the attractor gets stronger for larger values of ξ_ϕ . For a nonelliptical potential, in which the nonminimal couplings are equal ($\xi_\phi = \xi_\chi$), the attractor-strength parameter may be rewritten $\tilde{\Lambda}_\phi \xi_\phi = -[(g/\lambda_\phi) - 1]\xi_\phi$. Since the strength of the attractor is a characterization of the curvature of the potential in the adiabatic direction, we will use the combination $[(g/\lambda_\phi) - 1]\xi_\phi$ as the effective coupling strength, rather than g/λ_ϕ , when examining the Floquet charts for large ξ_ϕ . Figure 12 shows the 3-dimensional Floquet charts, in which one may see a convergence into a forest of densely packed, large-valued, almost parallel instability bands for large ξ_ϕ . We find substantially more efficient amplification of isocurvature modes for $\xi_\phi \gg 1$ than for the $\xi_\phi = 0$ case.

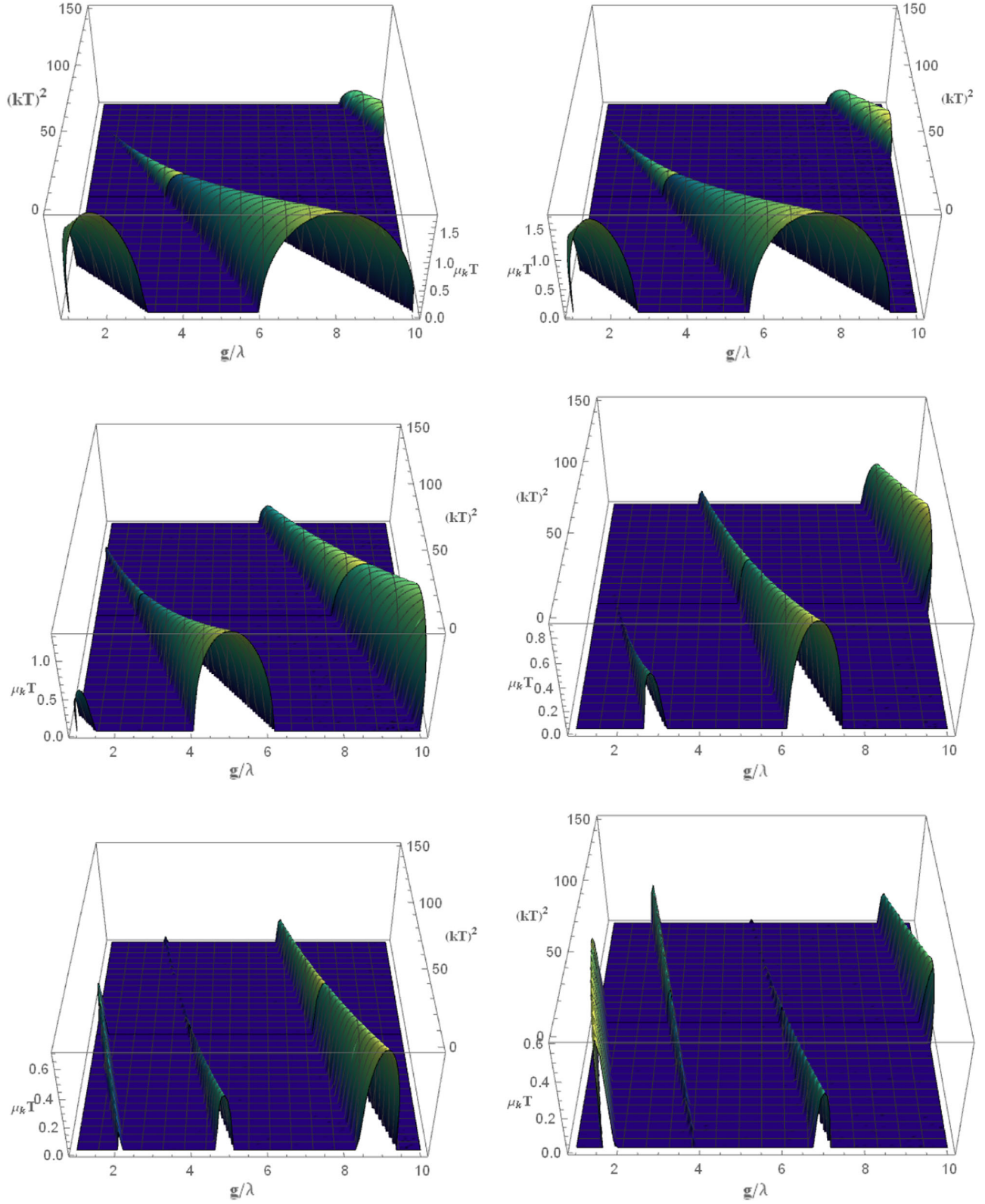


FIG. 11. Normalized Floquet exponents $\text{Re}[\mu_k]T$ for the isocurvature perturbations z_k as functions of g/λ and $(kT)^2$, for $\xi_\phi = \xi_\chi$. Top, left to right: $\xi_\phi = 0, 0.01$; middle, left to right: $\xi_\phi = 0.1, 0.4$; bottom, left to right: $\xi_\phi = 0.7, 1$. The bands are visibly tilting, shifting, and squeezing with increasing nonminimal coupling, indicating less efficient preheating for $\xi_\phi \sim \mathcal{O}(1)$ compared to the $\xi_\phi = 0$ case.

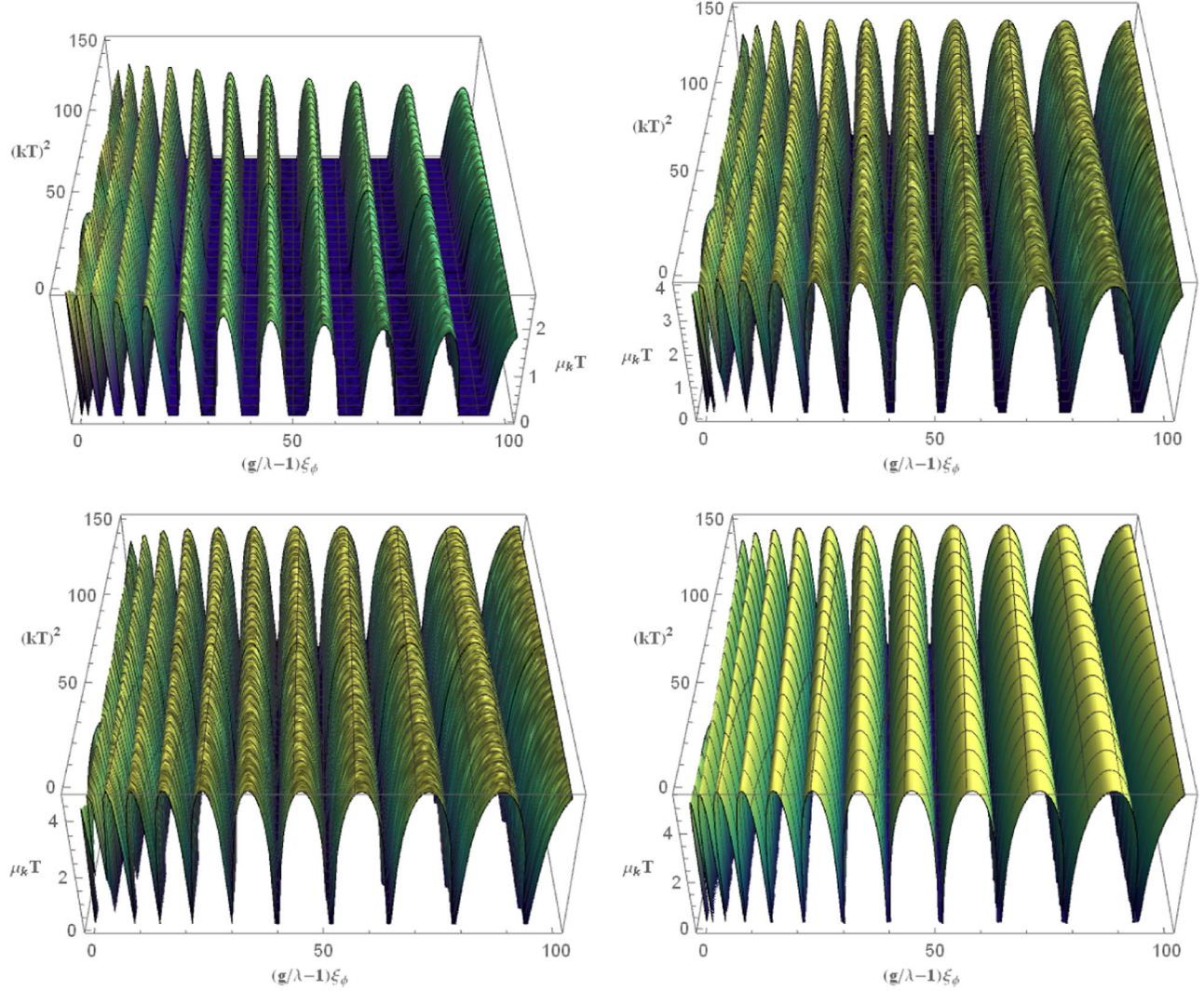


FIG. 12. Normalized Floquet exponents $\text{Re}[\mu_k]T$ for the isocurvature perturbations z_k , as functions of $[(g/\lambda_\phi) - 1]\xi_\phi$ and $(kT)^2$, for $\xi_\phi = \xi_\chi$. Top, left to right: $\xi_\phi = 10, 10^2$; bottom, left to right: $\xi_\phi = 10^3, 10^4$. The similarity of the Floquet charts for large ξ_ϕ is visible.

In order to more readily examine the structure of these Floquet charts, we present two-dimensional slices of them in Fig. 13, in which each panel shows the Floquet exponent for a specific rescaled wave number kT as a function of the effective coupling $[(g/\lambda_\phi) - 1]\xi_\phi$. There are several interesting points about the band structure in the regime of large nonminimal couplings. First, there is an increase of the value of $\text{Re}[\mu_k]$ as one increases the nonminimal coupling. The approach to an asymptotic solution is not as immediate as in the adiabatic case, though the $\xi_\phi = 10^4$ case differs from the $\xi_\phi = 10^5$ case only by about 10%. For $\xi_\phi = 10$ the value of $\text{Re}[\mu_k]$ is higher at lower effective coupling. This situation is reversed as one increases the nonminimal coupling: for large ξ_ϕ , nearly all bands have essentially the same height. Finally, from Fig. 13 we note that the bands tilt and become narrower for increasing k , though the effect only becomes pronounced for $kT \geq 10$.

In the large- ξ_I regime, we thus find a distinct behavior of the structure of the instability bands that has no analog in models with minimally coupled fields. Whereas our goal for this analysis has been to characterize the resonance structure, and note significant differences from previous, well-studied models, the behavior shown in Figs. 12 and 13 raises additional, interesting questions. In particular, as discussed in Ref. [88], the perturbative unitarity scale Λ for these models becomes a function of the inflaton amplitude. In the Einstein frame, in the limit $\xi_\phi \gg 1$, the strong-coupling scale Λ scales as M_{pl} during inflation (for $\phi \geq M_{\text{pl}}/\sqrt{\xi_\phi}$) before asymptoting to $\Lambda \sim M_{\text{pl}}/\xi_\phi$ for small field values ($\phi < M_{\text{pl}}/\xi_\phi$). Therefore one should take care that the wave numbers k under consideration do not extend into the regime $k > \Lambda$.

Within the rigid-spacetime approximation (which we adopt throughout this paper), the strong-coupling regime

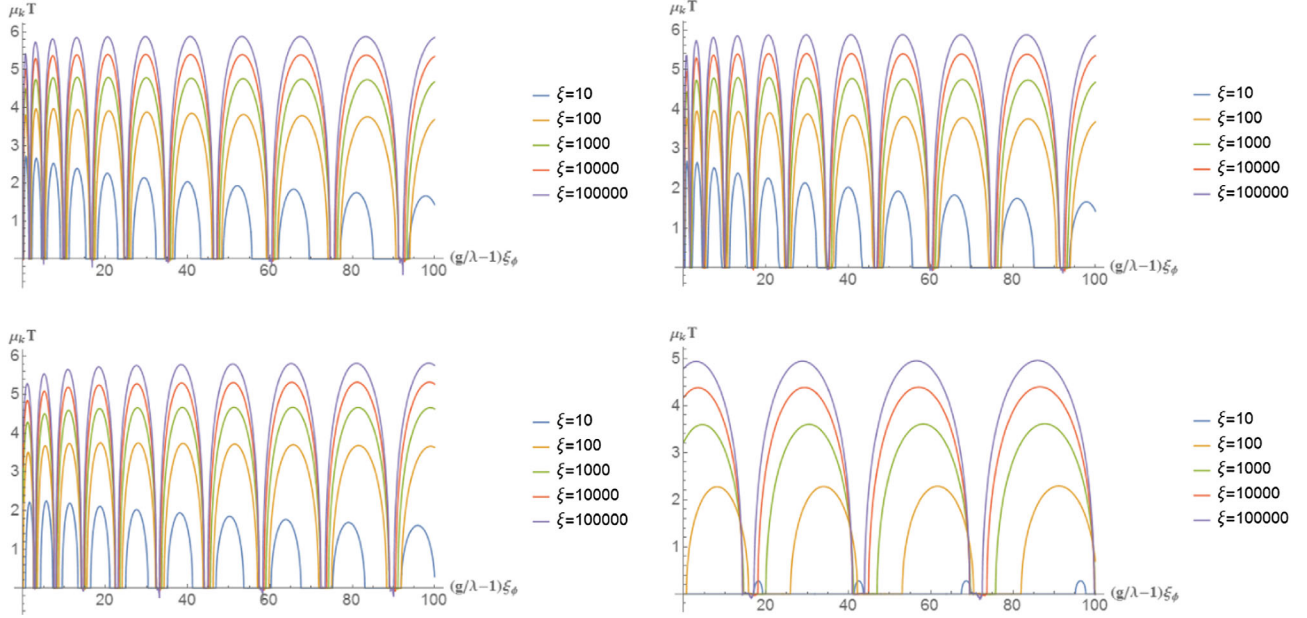


FIG. 13. Normalized Floquet exponents $\text{Re}[\mu_k]T$ for the isocurvature perturbations z_k , as functions of $[(g/\lambda_\phi) - 1]\xi_\phi$ and $(kT)^2$, for $\xi_\phi = \xi_\chi = 10, 10^2, 10^3, 10^4, 10^5$. Each two-dimensional plot corresponds to a slice through the full Floquet chart of Fig. 12 at a specific normalized wave number: top, left to right: $kT = 0, 1$; bottom, left to right: $kT = 10, 100$.

does not enter the analysis, since $\Lambda \propto M_{\text{pl}} \rightarrow \infty$; hence *every* mode with finite comoving wave number satisfies $k \ll \Lambda$. Moreover, even if we restore M_{pl} to its usual value, we find at the start of preheating, when $\phi \sim M_{\text{pl}}/\sqrt{\xi_\phi}$ and $\Lambda \sim M_{\text{pl}}$, that $k < \Lambda$ for $kT < 14.8\xi_\phi$, given that the inflaton period T scales as $T \simeq 14.8\xi_\phi/M_{\text{pl}}$ in the large- ξ_ℓ regime [1]. Later during preheating, as the amplitude of ϕ falls and $\Lambda \rightarrow M_{\text{pl}}/\xi_\phi$, we expect modes with $kT \lesssim 10$ to satisfy $k < \Lambda$. Of course, to fully explore the dynamics of the system beyond the linearized analysis we have pursued here, one would also need to consider particle rescatterings, from which large k modes could enter the strong-coupling regime. An analysis of the high- k behavior of these models beyond linear order in the perturbations remains beyond the scope of the present paper, and we leave potential implications of the strong-coupling regime for future research.

In sum, for the isocurvature modes z_k and symmetric nonminimal couplings ($\xi_\phi = \xi_\chi$), there is a weak convergence with increasing ξ_ϕ to an asymptotic solution that has large values of $\text{Re}[\mu_k]$ across dense, almost-parallel instability bands. The dense instability profile for the isocurvature modes for large ξ_ϕ is related to the rich spectral content of the background field for large ξ_ϕ , as identified in Figs. 3 and 4. We may make sense of the behavior shown in Figs. 11–13 semianalytically.

A. Small ξ_ϕ

As shown in Fig. 11, preheating into isocurvature modes becomes *less* efficient for $0 < \xi_\phi < 1$ compared to the minimally coupled case, with $\xi_\phi = 0$. We may understand

this trend qualitatively by returning to Fig. 4, which shows the amplitudes of the first few nonzero Fourier coefficients a_n of the background field's evolution. In the limit $\xi_\phi \rightarrow 0$, only the first two harmonics (a_2 and a_6) have any sizable amplitude, and the ratio between them is quite large, with $a_2/a_6 \sim 20$. As one approaches $\xi_\phi \rightarrow 1$ from below, one still finds only these two dominant harmonics, but the magnitude of a_6 falls relative to a_2 , such that the background field's oscillations become more nearly sinusoidal. With fewer nontrivial harmonics in the background field's evolution, the coupled perturbations experience fewer resonances, and the overall amplification falls. For $\xi_\phi > 1$, on the other hand, several harmonics begin to rise in magnitude, yielding the richer and more efficient resonance structure depicted in Figs. 12 and 13.

We may further understand properties of the Floquet charts by examining the Fourier structure of certain field-space quantities. In the rigid-spacetime limit, Eq. (22) for the isocurvature modes z_k may be written in the suggestive form

$$\frac{d}{dt} \begin{pmatrix} z_k \\ \dot{z}_k \end{pmatrix} = \begin{pmatrix} 0 & 1 \\ -(k^2 + m_{\text{eff},\chi}^2) & 0 \end{pmatrix} \begin{pmatrix} z_k \\ \dot{z}_k \end{pmatrix}, \quad (32)$$

again using $m_{\text{eff},\chi}^2 = m_{1,\chi}^2 + m_{2,\chi}^2$ in the rigid-spacetime limit. This equation is of the form

$$\dot{x}(t) = A(t)x(t), \quad (33)$$

where $A(t)$ is a periodic matrix with period $T/2$, and T is the period of the background-field oscillation. This allows us to

employ the machinery of Floquet theory to semianalytically study the boundaries that separate resonant from nonresonant regions in parameter space. In particular, at the boundaries between stable and unstable regions (at which $\text{Re}[\mu_k] = 0$), there exist $T/2$ -periodic and T -periodic solutions for $z_k(t)$.

We describe the method in Appendix B and summarize the results here. The stability boundaries for the isocurvature modes z_k are given implicitly by the equations

$$\begin{aligned}\det[Z((kT)^2, g/\lambda_\phi)] &= 0, \\ \det[\mathcal{Z}((kT)^2, g/\lambda_\phi)] &= 0, \\ \det[Z'((kT)^2, g/\lambda_\phi)] &= 0, \\ \det[\mathcal{Z}'((kT)^2, g/\lambda_\phi)] &= 0,\end{aligned}\quad (34)$$

where the matrices Z , \mathcal{Z} , Z' , and \mathcal{Z}' are functions of g/λ_ϕ and k . For example, the components of the matrix Z are given by

$$\begin{aligned}Z_{00} &= k^2 + b_{k,0}, \\ Z_{p,p} &= -4p^2\omega^2 + k^2 + b_{k,0} + \frac{1}{2}b_{k,2p}, \quad p \geq 1, \\ Z_{p,q} &= \frac{1}{2}(b_{k,|p-q|} + b_{k,p+q}), \quad p \neq q,\end{aligned}\quad (35)$$

where $\omega = 2\pi/T$ and $b_{k,p}$ are the coefficients of a (cosine) Fourier expansion of $\Omega_{(\chi)}^2(k, t)$. The related Z' , \mathcal{Z} , and \mathcal{Z}' matrices are constructed in Appendix B. There are four matrices altogether for the isocurvature modes, arising from sine and cosine Fourier expansions for both the $T/2$ - and T -periodic solutions.

Solving the equations in Eq. (34) would give exact (implicit) equations for the boundaries of all stable regions, but—since these matrices are infinite dimensional—doing so is computationally intractable. However, by truncating these matrices at an appropriate order we may understand the origin of the band-tilting with increasing ξ_ϕ . In particular, as demonstrated in Appendix B, truncating to 3×3 matrices provides sufficiently accurate approximations with which to understand the shift of the boundaries of the fundamental instability band. (For higher-order instability bands, one may truncate the matrices to sizes larger than 3×3 , though understanding the behavior of the fundamental instability band will suffice for our purposes.)

For small ξ_ϕ , the boundaries of the regions $\text{Re}[\mu_k] = 0$ are approximately linear in the $(kT)^2$ -versus- g/λ_ϕ plane, which means that the slope is approximately constant everywhere along a given boundary. The intercepts along the $(kT)^2$ axis are the solutions to the determinant equations of Eq. (34) with $g/\lambda_\phi = 0$, and those along the g/λ_ϕ axis are the solutions with $(kT)^2 = 0$. Since all of the relevant matrices depend only on the Fourier coefficients of $m_{\text{eff},\chi}^2$, the change in slope of the $\text{Re}[\mu_k] = 0$ boundary in

the $(kT)^2$ - (g/λ_ϕ) plane—which we call “band tilting”—may be determined analytically by calculating the Fourier coefficients of $dm_{\text{eff},\chi}^2/d\xi_\phi$.

We write the contributions to $m_{\text{eff},\chi}^2$ in a suggestive form, in which we isolate the dependence on the coupling parameter g :

$$\begin{aligned}m_{1,\chi}^2 &= \left\{ \frac{g\delta^2}{\xi_\phi(\delta^2+1)^2} - \frac{\delta^4(\delta^2(6\xi_\phi+1)+6\xi_\phi+2)}{(\delta^2+1)^3\xi_\phi(\delta^2(6\xi_\phi+1)+1)} \right\} M_{\text{pl}}^2, \\ m_{2,\chi}^2 &= \frac{2\dot{\delta}^2(\delta^2(6\xi_\phi+1)+3\xi_\phi+1)}{(\delta^2+1)^2(\delta^2(6\xi_\phi+1)+1)} M_{\text{pl}}^2,\end{aligned}\quad (36)$$

where again we use $\delta \equiv \sqrt{\xi_\phi}\phi/M_{\text{pl}}$. In order to isolate the band-tilting effect, we study one particular stability band, which we call the *primary stability band*: the large central band in the first Floquet chart in Fig. 11. We consider how the upper stability boundary shifts with changing ξ_ϕ . (Similar results may be obtained for the other stability boundaries.) For $\xi_\phi = 0$, the upper stability boundary has a slope in the $(kT)^2$ - g/λ_ϕ plane of about 15; as ξ_ϕ increases toward 1, the slope rises sharply to roughly 100, as shown on the left in Fig. 14. This band-tilting effect is consistent with the features displayed in the Floquet charts of Fig. 11.

Another effect displayed in the Floquet charts in Fig. 11 is that the bands become narrower as ξ_ϕ increases. Again we focus on the primary instability band, and consider its upper and lower boundaries. The width of the band, Δ , can be quantified by the difference between the g/λ_ϕ intercepts of the upper and lower stability boundaries. The narrowing of Δ with increasing ξ_ϕ is shown on the right in Fig. 14, which again agrees with the results of Fig. 11.

B. Large ξ_ϕ

For large ξ_ϕ , we again consider Eqs. (32) and (36), but now examine how the distinct contributions to $m_{\text{eff},\chi}^2$ scale with ξ_ϕ . We begin with $m_{2,\chi}^2$ and consider the behavior for $\xi_\phi \gg 1$ and $\delta \neq 0$:

$$\frac{m_{2,\chi}^2}{M_{\text{pl}}^2} = \left(\frac{2\delta^2+1}{\delta^2(\delta^2+1)^2} + \mathcal{O}(\xi_\phi^{-1}) \right) \dot{\delta}^2 \sim \frac{1}{\xi_\phi^2}, \quad (37)$$

since $\dot{\delta}$ scales like $1/\xi_\phi$ if we change the time variable to $t \rightarrow \tilde{t} = \sqrt{\lambda_\phi} M_{\text{pl}} t / \xi_\phi$. Using the same dimensional arguments for $m_{1,\chi}^2$ we find

$$\frac{m_{1,\chi}^2}{M_{\text{pl}}^2} = \frac{\delta^2[(g/\lambda_\phi) - 1]}{(\delta^2+1)^2\xi_\phi} + \mathcal{O}(\xi_\phi^{-2}). \quad (38)$$

Equations (37) and (38) reveal different scaling for the two components of $m_{\text{eff},\chi}^2$, which makes the analysis of the isocurvature modes in the large- ξ_ϕ regime more difficult than for the adiabatic modes. Furthermore, the two components of

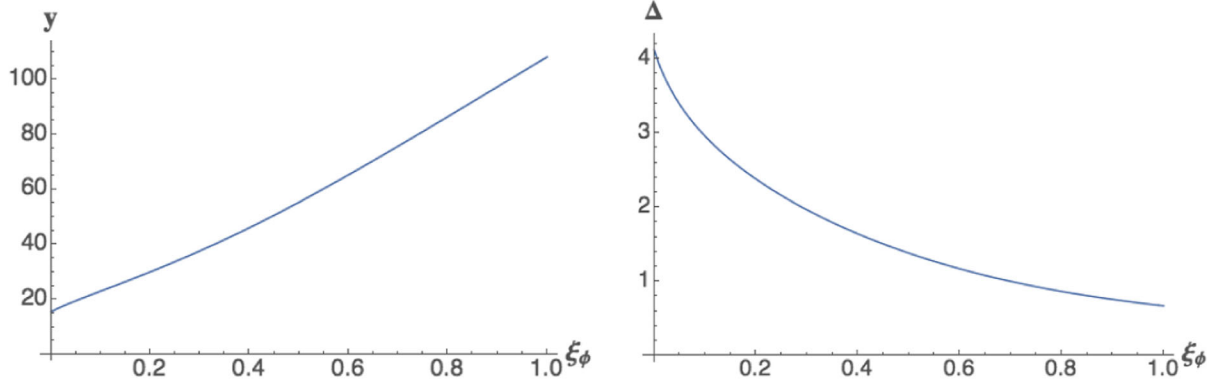


FIG. 14. Left: slope y of the upper boundary of the primary stability band as a function of ξ_ϕ for $0 \leq \xi \leq 1$. This plot shows that stability bands tilt upward in the $(kT)^2$ - (g/λ_ϕ) plane as ξ_ϕ increases. Right: width of the primary instability band Δ as a function of ξ_ϕ , where Δ is defined as the difference between the g/λ_ϕ intercepts of the upper and lower stability boundaries.

$m_{\text{eff},\chi}^2$ oscillate out of phase, since one is proportional to δ^2 and the other to $\dot{\delta}^2$. Their distinct scaling with ξ_ϕ controls the features of $m_{\text{eff},\chi}^2$, such as when it has sharp features and when it crosses zero. (See also Refs. [1,79].)

We demonstrated in Ref. [1] that the attractor behavior along the $\chi = 0$ direction is controlled by the combination $\tilde{\Lambda}_\phi \xi_\phi$, which (as we saw in Figs. 12 and 13) is also the effective coupling that makes the Floquet charts exhibit self-similar scaling behavior in the large- ξ_ϕ limit. For the case $\xi_\phi = \xi_\chi$ (zero ellipticity), we may perform a change of variables

$$\frac{g}{\lambda_\phi} = 1 - \tilde{\Lambda}_\phi = 1 + \frac{a_\phi}{\xi_\phi}, \quad (39)$$

where we have introduced the parameter $a_\phi \equiv -\tilde{\Lambda}_\phi \xi_\phi$. [Recall that the attractor along $\chi = 0$ corresponds to $\tilde{\Lambda}_\phi < 0$; here a_ϕ is chosen to denote the word “attractor,” and should not be confused with either the scale factor $a(t)$ or the Fourier coefficients a_n .] The parameter a_ϕ is proportional to the parameter $\kappa \equiv 4(\lambda_\phi \xi_\chi - g \xi_\phi)/\lambda_\phi$ defined in Ref. [26], which was introduced to study the evolution of isocurvature perturbations during inflation along the top of a ridge in the potential; here we will use a_ϕ to study preheating of isocurvature modes within a valley of the potential.

Using the attractor parameter a_ϕ , the term $m_{1,\chi}^2$ in Eq. (36) may be written

$$\begin{aligned} \frac{m_{1,\chi}^2}{M_{\text{pl}}^2} &= \frac{\delta^2(\xi_\phi - a_\phi(\delta^2 + 1)(\delta^2(6\xi_\phi + 1) + 1))}{(\delta^2 + 1)^3 \xi_\phi^2 (\delta^2(6\xi_\phi + 1) + 1)} \\ &= \frac{1 - 6a_\phi(\delta^4 + \delta^2)}{6(\delta^2 + 1)^3 \xi_\phi^2} + \mathcal{O}(\xi_\phi^{-3}). \end{aligned} \quad (40)$$

We can therefore distinguish three distinct regimes of parameters relevant to the analysis of $m_{\text{eff},\chi}^2$ for the isocurvature perturbations, all within the limit of zero ellipticity

($\xi_\phi = \xi_\chi$): a symmetric potential, with $g = \lambda_\phi$ and hence $a_\phi = 0$; a softly broken symmetry, with $|\tilde{\Lambda}_\phi| \sim \xi_\phi^{-1} \ll 1$ and hence $a_\phi \sim \mathcal{O}(1)$; and a generic potential, with $|\tilde{\Lambda}_\phi| \sim \mathcal{O}(1)$ and hence $a_\phi \sim \xi_\phi$. For $a_\phi \sim \mathcal{O}(1)$, we find $m_{1,\chi}^2 \sim m_{2,\chi}^2 \sim \xi_\phi^{-2}$, whereas for $a_\phi \gg 1$ we have $m_{1,\chi}^2 \sim \xi_\phi^{-1}$ and $m_{2,\chi}^2 \sim \xi_\phi^{-2}$.

1. Symmetric potential, $a_\phi = 0$

An interesting case is that of a symmetric potential, with $\xi_\phi = \xi_\chi$ and $g = \lambda_\phi = \lambda_\chi$ (and hence $a_\phi = 0$). Apart from its simplicity, the symmetric case is relevant to models like Higgs inflation [16,24]. (For the Higgs inflation case there are three identical isocurvature modes [24], but this does not change our analysis.) Figure 15 shows the behavior of the rescaled effective masses $\tilde{m}_{\text{eff}}^2 = \xi_\phi^2 m_{\text{eff}}^2$ for the adiabatic and isocurvature modes, for $\xi_\phi \gg 1$. We note that the sharp features in $\tilde{m}_{\text{eff},\phi}^2$ that we identified in Fig. 6 are swamped by the spikes in $\tilde{m}_{\text{eff},\chi}^2$ in the limit $\xi_\phi \gg 1$ (a trend

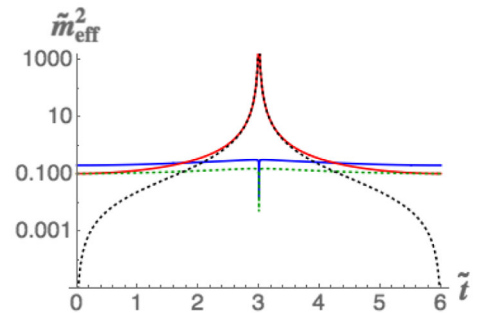


FIG. 15. The rescaled effective masses, $\tilde{m}_{\text{eff}}^2 = \xi_\phi^2 m_{\text{eff}}^2$, for the adiabatic (blue) and isocurvature (red) modes (in units of M_{pl}) versus $\tilde{t} = \sqrt{\lambda_\phi} M_{\text{pl}} t / \xi_\phi$, for a symmetric potential ($\xi_\phi = \xi_\chi$, $g = \lambda_\phi = \lambda_\chi$), with $\xi_\phi = 10^3$. The green and black dashed curves show the contributions to $\tilde{m}_{\text{eff},\chi}^2$ arising from the potential ($\tilde{m}_{1,\chi}^2$) and from the nontrivial field-space manifold ($\tilde{m}_{2,\chi}^2$), respectively.

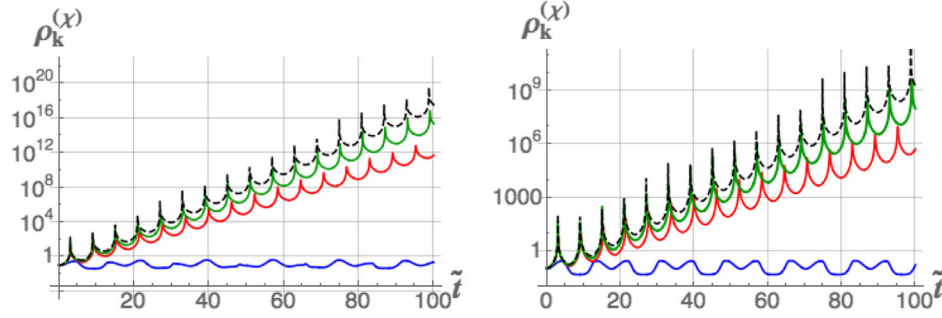


FIG. 16. Energy density $\rho_k^{(\chi)}$ for the isocurvature modes z_k in a symmetric potential ($\xi_\phi = \xi_\chi$, $g = \lambda_\phi = \lambda_\chi$), as a function of $\tilde{t} = \sqrt{\lambda_\phi} M_{\text{pl}} t / \xi_\phi$. The wave numbers are $\tilde{k} = 0$ (left) and $\tilde{k} = 0.1$ (right), with $\tilde{k} = k \xi_\phi / (\sqrt{\lambda_\phi} M_{\text{pl}})$. In both plots, the nonminimal couplings are given by $\xi_\phi = 10, 10^2, 10^3, 10^4$ (bottom to top: blue, red, green, black dashed, respectively). Compare with the growth of adiabatic modes shown in Figs. 8 and 9.

also noted in Ref. [79]). In particular, the spikes of $\tilde{m}_{\text{eff},\chi}^2$ for $\xi_\phi \gg 1$ arise from the nontrivial field-space manifold ($\tilde{m}_{2,\chi}^2$) rather than from the potential ($\tilde{m}_{1,\chi}^2$), and hence have no analog in the minimally coupled case.

The energy density of the isocurvature modes likewise quickly exceeds that of the adiabatic modes in the large- ξ_ϕ limit. In Fig. 16 we plot $\rho_k^{(\chi)}$ for the case of symmetric couplings, for various values of ξ_ϕ and two distinct modes k . We note first the sensitivity to wave number: both modes shown here become amplified exponentially quickly, but the $k = 0$ mode grows even more quickly than the $k \xi_\phi = 0.1$ mode. For both modes, we find no particular growth for $\xi_\phi = 10$, and then a convergence toward a single large- ξ_ϕ behavior for $\xi_\phi \geq 100$. Compare with the more modest amplification of the adiabatic modes for $\xi_\phi \gg 1$ shown in Figs. 8 and 9. (As in our analysis of the adiabatic modes, we neglect nonlinear effects such as backreaction; our goal is to understand the earliest phases of the preheating resonances.)

2. Softly broken symmetry, $a_\phi \sim \mathcal{O}(1)$

For the case of a softly broken symmetry, with $|\tilde{\Lambda}_\phi| \ll 1$ and hence $a_\phi \sim \mathcal{O}(1)$, we find that the isocurvature modes $z_k(t)$ oscillate more times per background oscillation for larger values of a_ϕ , as shown in Fig. 17. This means that the system can move from the narrow- to the broad-resonance regime [42], in which the (normalized) effective mass of the isocurvature modes becomes large. The system exits the regime of softly broken symmetry once a_ϕ becomes comparable to ξ_ϕ .

Figure 18 shows the isocurvature effective mass for $\xi_\phi = 10^4$ and varying a_ϕ (or equivalently varying g/λ_ϕ). As expected, the spike does not change, since it arises from the nontrivial field-space manifold ($\tilde{m}_{2,\chi}^2$) rather than from the potential ($\tilde{m}_{1,\chi}^2$), and hence is independent of g/λ_ϕ . The potential contribution $\tilde{m}_{1,\chi}^2$ grows with growing g/λ_ϕ ,

leading the system from narrow to broad resonance as $\tilde{m}_{\text{eff},\chi}$ becomes larger than the background frequency. By keeping a_ϕ fixed and varying ξ_ϕ , we see that the spike in the isocurvature effective mass becomes more pronounced for larger values of the nonminimal coupling. In the case of $\xi_\phi = 10$ there is no sharp feature, since the two components of the isocurvature effective mass are similar in magnitude and opposite in phase. We thus see again the clear distinction between the intermediate- and large- ξ_ϕ regime in the context of preheating. These trends are reinforced in Fig. 19, which depicts the different contributions to $\tilde{m}_{\text{eff},\chi}^2$ from $\tilde{m}_{1,\chi}^2$ and $\tilde{m}_{2,\chi}^2$, and the dependence of $\rho_k^{(\chi)}$ on a_ϕ and ξ_ϕ for the softly broken symmetry case.

3. Arbitrary valley, $a_\phi \sim \xi_\phi$

We now consider a generic potential, meaning that $g/\lambda_\phi \sim \mathcal{O}(1)$ has some arbitrary value (different from $g/\lambda_\phi = 1$, which corresponds to the symmetric case). We will use $g/\lambda_\phi = 2$ for definiteness. In this case, $a_\phi \sim \xi_\phi \gg 1$.

The isocurvature effective mass is shown in Fig. 20 for a range of nonminimal couplings. We can see that the overall magnitude of $\tilde{m}_{\text{eff},\chi}^2$ increases with increasing ξ_ϕ for a fixed

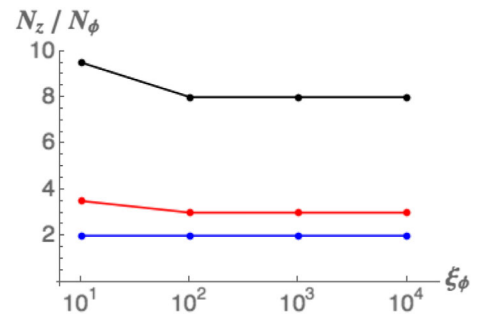


FIG. 17. The number of times the isocurvature mode $z_k(t)$ with $k = 0$ oscillates per background oscillation (N_z/N_ϕ) as a function of a_ϕ and ξ_ϕ , where $g/\lambda_\phi = 1 + (a_\phi/\xi_\phi)$: $a_\phi = 2$ (blue), $a_\phi = 20$ (red), and $a_\phi = 200$ (black), from bottom to top.

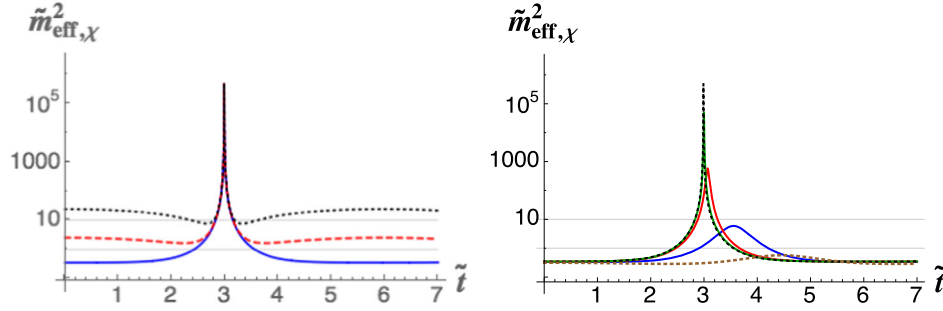


FIG. 18. Left: rescaled effective mass for the isocurvature modes $\tilde{m}_{\text{eff},\chi}^2 = \xi_\phi^2 m_{\text{eff},\chi}^2$ (in units of M_{pl}) versus $\tilde{t} = \sqrt{\lambda_\phi} M_{\text{pl}} t / \xi_\phi$ for a softly broken symmetric potential with $\xi_\phi = \xi_\chi = 10^4$ and $g/\lambda_\phi = 1 + (2/\xi_\phi)$ (blue), $g/\lambda_\phi = 1 + (20/\xi_\phi)$ (red-dashed), and $g/\lambda_\phi = 1 + (200/\xi_\phi)$ (black-dotted). Right: effective mass $\tilde{m}_{\text{eff},\chi}^2$ for $g/\lambda_\phi = 1 + (2/\xi_\phi)$ and $\xi_\phi = 3, 10, 10^2, 10^3, 10^4$ (brown, blue, red, green, and black, respectively).

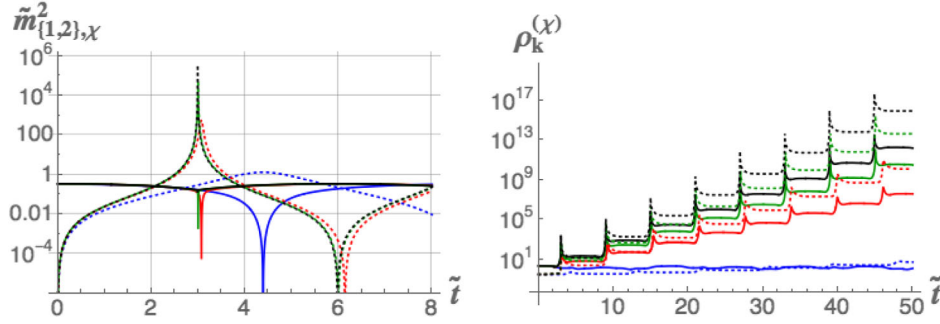


FIG. 19. Left: contributions $\tilde{m}_{\{1,2\},\chi}^2 = \xi_\phi^2 m_{\{1,2\},\chi}^2$ to $\tilde{m}_{\text{eff},\chi}^2$ versus $\tilde{t} = \sqrt{\lambda_\phi} M_{\text{pl}} t / \xi_\phi$ for a softly broken symmetric potential with $\xi_\phi = \xi_\chi$, $g/\lambda_\phi = 1 + (a_\phi/\xi_\phi)$, and $a_\phi = 2$. Solid lines correspond to the contributions that arise from the potential ($\tilde{m}_{1,\chi}^2$) and dotted lines correspond to the contributions that arise from the nontrivial field-space manifold ($\tilde{m}_{2,\chi}^2$). Right: energy density $\rho_k^{(\chi)}$ for $k = 0$ and $\xi_\phi = \xi_\chi$, with $g/\lambda_\phi = 1 + (a_\phi/\xi_\phi)$ and $a_\phi = 2$ (dotted line) and $a_\phi = 20$ (solid line). In both plots, the nonminimal couplings are given by $\xi_\phi = 10, 10^2, 10^3, 10^4$ (blue, red, green, and black, respectively).

value of g/λ_ϕ . This is easily understood. For $\delta \neq 0$ the velocity is $\dot{\delta} \sim 0$; hence the potential term dominates: $\tilde{m}_{1,\chi}^2 \gg \tilde{m}_{2,\chi}^2$. For $a_\phi \sim \xi_\phi$, we found above that $m_{1,\chi}^2 \sim \xi_\phi^{-1}$, and hence $\tilde{m}_{1,\chi}^2 = \xi_\phi^2 m_{1,\chi}^2 \sim \xi_\phi$, consistent with the behavior shown in Fig. 20 away from the spike. Thus larger ξ_ϕ values lead to larger masses for the isocurvature perturbations. On the other

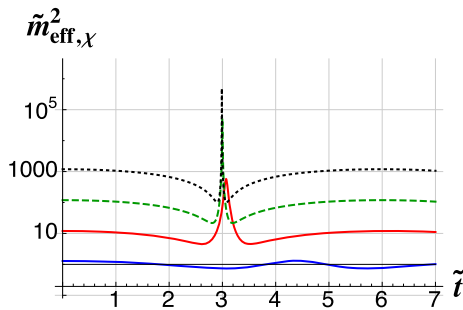


FIG. 20. The rescaled effective mass $\tilde{m}_{\text{eff},\chi}^2$ versus $\tilde{t} = \sqrt{\lambda_\phi} M_{\text{pl}} t / \xi_\phi$ for $g/\lambda_\phi = 2$ (or $a_\phi = \xi_\phi$), and $\xi_\phi = 10, 10^2, 10^3, 10^4$ (bottom to top: blue, red, green-dashed, and black-dotted, respectively).

hand, for $\xi_\phi \sim \mathcal{O}(10)$, $\max(m_{1,\chi}^2) \sim \max(m_{2,\chi}^2)$ but with the two terms out of phase with each other, so $\tilde{m}_{\text{eff},\chi}^2$ does not develop sharp features and the modes $z_k(t)$ do not undergo rapid amplification.

Since we have rescaled time as $\tilde{t} = \sqrt{\lambda_\phi} M_{\text{pl}} t / \xi_\phi$, the background field's oscillation period for $\xi_\phi \gg 1$ is given by $\tilde{T} = T/\xi_\phi \simeq 14.8$ [in units of $(\sqrt{\lambda_\phi} M_{\text{pl}})^{-1}$]. As shown in Fig. 21, larger values for the isocurvature mass put the system into the broad-resonance regime [42], in the sense that the fluctuations oscillate multiple times for each background oscillation, with correspondingly rapid growth of $\rho_k^{(\chi)}$.

4. Varying ellipticity

For completeness we construct the Floquet charts for elliptical potentials, with $\xi_\phi \neq \xi_\chi$. In Ref. [26] we introduced the ellipticity parameter $\varepsilon \equiv (\xi_\phi - \xi_\chi)/\xi_\phi$. Figure 22 shows the resulting instability bands for varying ellipticity. We fix $\xi_\phi = 10^4$, which is well into the regime of large nonminimal coupling. For positive ellipticity, meaning $\xi_\chi < \xi_\phi$, the instability bands become larger both in

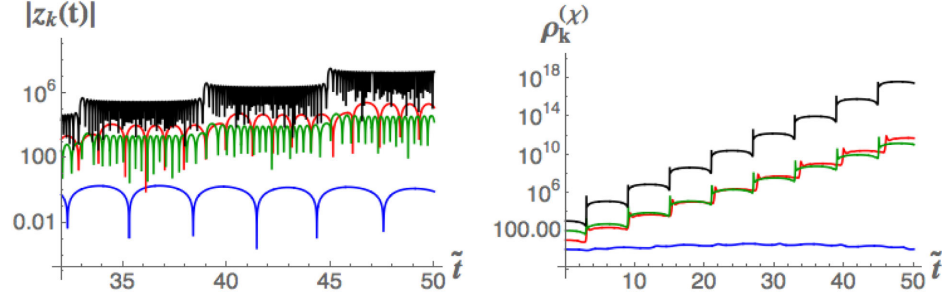


FIG. 21. Left: amplitude of the isocurvature mode $|z_k(t)|$ for $k = 0$, with $g/\lambda_\phi = 2$ and varying ξ_ϕ . Note that as ξ_ϕ increases, $z_k(t)$ oscillates more frequently per oscillation of the background field, entering the broad-resonance regime. Right: isocurvature energy density $\rho_k^{(x)}$ for $k = 0$ and $g/\lambda_\phi = 2$. For both plots, $\xi_\phi = 10, 10^2, 10^3, 10^4$ (bottom to top: blue, red, green, and black, respectively).

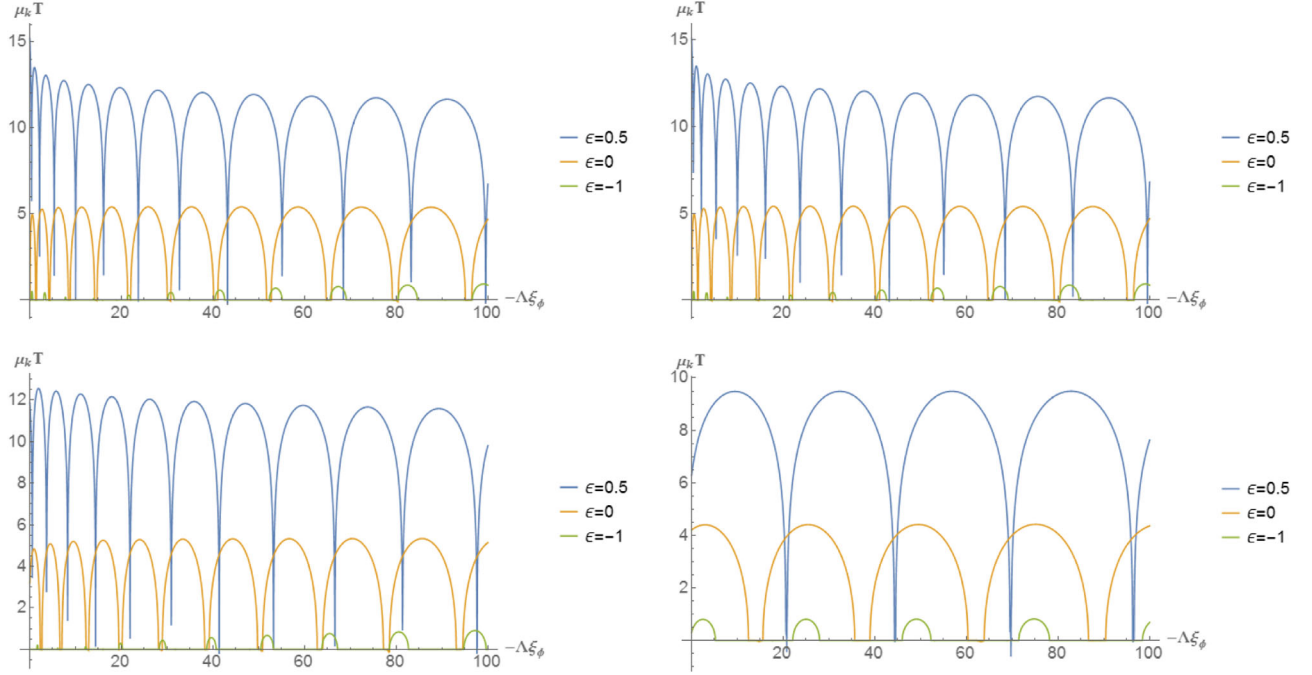


FIG. 22. Floquet exponents for the isocurvature perturbations normalized by the period of background oscillations for $\xi_\phi = 10^4$ and varying $\epsilon = 0.5, 0, -1$. Each two-dimensional plot corresponds to a slice of the full Floquet chart at a specific normalized wave number: top, left to right: $kT = 0, 1$; bottom, left to right: $kT = 10, 100$.

amplitude and width. The opposite occurs for negative ellipticity, with $\xi_\chi > \xi_\phi$, for which the instability bands become suppressed and further apart. For $\xi_\chi = 2\xi_\phi$ (or $\epsilon = -1$), the resonances vanish for most values of the effective coupling $-\Lambda_\phi \xi_\phi$. This behavior during preheating is reminiscent of the behavior of these systems during inflation [26], for which the fraction of isocurvature modes produced, β_{iso} , is enhanced for positive ellipticity and suppressed for negative ellipticity [103].

VI. CONCLUSIONS

Using the covariant formalism developed in Ref. [1], in this paper we have investigated the resonance structure for the amplification of adiabatic and isocurvature

perturbations during preheating in models with multiple scalar fields nonminimally coupled to gravity. In these models, the background dynamics generically fall into a single-field attractor that persists (at least) through the preheating phase [1], thereby avoiding the “dephasing” [80,81] that commonly occurs in multifield models with minimal couplings. Within the approximation of a rigid spacetime, we identified several unique features of the preheating dynamics that arise due to the nontrivial field-space manifold, which have no analog in minimally coupled models.

For nonminimal couplings $\xi_I \geq \mathcal{O}(1)$, the spectral content of the background field differs significantly from its minimally coupled counterpart, the well-known quartic model. Whereas in the case of the minimally coupled

quartic model the background dynamics may be well described by the first two harmonics, in the presence of nonminimal couplings, higher harmonics attain comparable magnitude to the lowest harmonics. Furthermore, for a specific combination of the field's amplitude and non-minimal coupling, all but the fundamental harmonic vanish, giving a simple sinusoidal solution. For large nonminimal couplings, the ratios of the Fourier coefficients for various harmonics quickly asymptote to fixed values, such that for $\xi_\phi > \mathcal{O}(100)$ the spectral content of the background inflaton field is independent of the exact value of ξ_ϕ .

The behavior of the adiabatic and isocurvature perturbations is very different. For the adiabatic modes, the Floquet charts for small nonminimal couplings present a dominant, primary instability band at nonzero values of the wave number. This is completely reversed for large non-minimal couplings, for which the primary instability band occurs for $k \sim 0$, making the two cases—small and large nonminimal coupling—qualitatively distinct. Furthermore, for large nonminimal coupling $\xi_\phi \gtrsim 10^3$, the Floquet chart quickly asymptotes to a common shape, yielding a single scaling behavior for the adiabatic perturbations in the limit of large ξ_I .

The isocurvature modes show richer phenomenology, since their behavior also depends on the coupling between the two fields ϕ and χ . For small values of the nonminimal coupling the Floquet chart resembles the Lamé chart, arising in the study of a minimally coupled quartic model. As the value of the nonminimal coupling increases, the instability bands tilt and become narrower, thus making preheating less efficient for $0 < \xi_I < 1$ compared to the case with $\xi_I = 0$. For large values of the nonminimal coupling, on the other hand, the Floquet chart is comprised of a dense set of closely spaced, almost parallel instability bands, making the amplification of isocurvature modes very efficient. Furthermore, the scaling solution found in the adiabatic case is also present for isocurvature modes, although the single behavior in the $\xi_I \rightarrow \infty$ limit is reached more slowly with increasing ξ_I than in the adiabatic case.

Finally, the preheating dynamics for both adiabatic and isocurvature modes reveal an intermediate region, for $\xi_I \sim \mathcal{O}(1-10)$. Within this intermediate region, the resonance structure for both adiabatic and isocurvature modes shows sensitive dependence on wave number and couplings, distinct from the minimally coupled case while also quite different from the behavior for $\xi_I \geq 10^2$. The emergence of this intermediate region during preheating is distinct from the behavior of spectral observables during inflation, such as the spectral index (n_s) and tensor-to-scalar ratio (r), which attain their large- ξ_I values for $\xi_I \gtrsim \mathcal{O}(10)$ [23–26]. Thus postinflation dynamics might provide one means of breaking the observational degeneracy of this class of models, even given the strong single-field attractor behavior during and after inflation.

Our aim in the present paper has been to understand how the resonance structure for this class of models changes

with the strength of the nonminimal couplings, within the rigid-spacetime approximation. We have therefore focused on the early preheating phase of reheating, working to linear order in the fluctuations and neglecting significant nonlinear effects such as backreaction from produced particles. We have found efficient resonance for $\xi_I \geq \mathcal{O}(100)$. In Ref. [2] we relax the assumption of a rigid spacetime, and consider some possible observational consequences of such an efficient preheating phase.

ACKNOWLEDGMENTS

It is a pleasure to thank Mustafa Amin, Bruce Bassett, Jolyon Bloomfield, Peter Fisher, Tom Giblin, Alan Guth, Mark Hertzberg, Johanna Karouby, and an anonymous referee for helpful discussions. We would like to acknowledge support from the Center for Theoretical Physics at MIT. This work is supported by the U.S. Department of Energy under grant Contract No. DE-SC0012567. M. P. D. and A. P. were also supported in part by MIT's Undergraduate Research Opportunities Program (UROP). C. P. W. thanks the University of Washington College of Arts & Sciences for financial support. She also gratefully acknowledges support from the MIT Dr. Martin Luther King, Jr. Visiting Professors and Scholars program and its director Edmund Bertschinger. E. I. S. gratefully acknowledges support from a Fortner Fellowship at the University of Illinois at Urbana-Champaign.

APPENDIX A: ASYMPTOTIC EQUATION OF MOTION

Starting from Eq. (13) and performing the following change of variables:

$$x = \log(1 + \delta^2), \quad (\text{A1})$$

the term including the first derivative vanishes and the resulting equation is

$$\ddot{x} + \frac{1}{3}e^{-2x}(e^x - 1) = 0, \quad (\text{A2})$$

where we work in terms of $\tilde{t} = \sqrt{\lambda_\phi} M_{\text{pl}} t / \xi_\phi$ and overdots denote $d/\tilde{d}\tilde{t}$. Equation (A2) is an analytically solvable asymptotic equation of motion which may be integrated in two steps. The first integration yields

$$\dot{x} dx = \frac{1}{3}e^{-2x}(1 - e^x)dx, \quad (\text{A3})$$

which integrates to

$$\dot{x} = \sqrt{2\left(C + \frac{1}{3}e^{-x} - \frac{1}{6}e^{-2x}\right)}. \quad (\text{A4})$$

The constant of integration C is defined by setting $\dot{x} = 0$ for $x = \log(1 + \alpha^2)$, where α is defined via $\phi_{\max} = \alpha M_{\text{pl}} / \sqrt{\xi_\phi}$, where ϕ_{\max} is the maximum field amplitude during the oscillation phase. By matching to the inflationary solution near \tilde{t}_{end} , α is constrained to $\alpha \leq 0.8$. Equation (A4) may then be integrated:

$$\frac{e^x \sqrt{6C + e^{-2x}(2e^x - 1)} \ln[1 + 6Ce^x + \sqrt{(6C)(6Ce^{2x} + 2e^x - 1)}]}{\sqrt{(2C)(6Ce^{2x} + 2e^x - 1)}} = \tilde{t} + C. \quad (\text{A5})$$

The new integration constant C may be determined by setting $x(0) = \log(1 + \alpha^2)$. Finally we may revert to our original variable by using $x = \log(\delta^2 + 1)$ and $\delta = \sqrt{\xi_\phi} \phi / M_{\text{pl}}$.

This is anything but a simple formula, and it cannot be analytically inverted to give $\delta(\tilde{t})$. Nonetheless, we have demonstrated the existence of an oscillatory solution whose behavior is independent of ξ_ϕ in the limit $\xi_\phi \rightarrow \infty$. Hence we may solve the asymptotic equation of motion (with no ambiguity about the value of ξ_ϕ) and calculate $\delta(\tilde{t})$ numerically, as in Sec. II B. The spectrum of $\delta(\tilde{t})$ is easily derived and compared with the spectrum of $\phi(\tilde{t})$ for finite values of ξ_ϕ , as in Fig. 4, showing excellent agreement for $\xi_\phi \gg 1$.

APPENDIX B: SEMIANALYTIC CALCULATION OF FLOQUET-BAND BOUNDARIES

In this appendix we construct infinite-dimensional matrices, whose vanishing determinants may be used to determine the stability boundaries, where $\text{Re}[\mu_k] = 0$, for both adiabatic and isocurvature modes. We also demonstrate that the characteristics of the boundary for the primary instability band may be determined with sufficient accuracy by truncating the matrices to simpler 3×3 form.

1. $T/2$ -periodic solutions

For convenience we define $\omega' \equiv 4\pi/T = 2\omega$, where T is the period of the background field's oscillations. We may then make the following expansions for the mode functions and their effective frequencies:

$$\begin{aligned} v_k &= \sum_{j=0}^{\infty} \alpha_{k,j} \cos 2j\omega t, \\ z_k &= \sum_{j=0}^{\infty} \beta_{k,j} \cos 2j\omega t, \\ \Omega_{(\phi)}^2 &= k^2 + a_{k,0} + \sum_{j=1}^{\infty} a_{k,j} \cos 2j\omega t, \\ a_{k,j} &= \left(1 - \frac{\delta_{j,0}}{2}\right) \frac{4}{T} \int_0^{T/2} m_{\text{eff},\phi}^2 \cos 2j\omega t, \\ \Omega_{(\chi)}^2 &= k^2 + b_{k,0} + \sum_{j=1}^{\infty} b_{k,j} \cos 2j\omega t, \\ b_{k,j} &= \left(1 - \frac{\delta_{j,0}}{2}\right) \frac{4}{T} \int_0^{T/2} m_{\text{eff},\chi}^2 \cos 2j\omega t. \end{aligned} \quad (\text{B1})$$

Plugging these relations into the equation of motion for the adiabatic modes, v_k , in Eq. (22) (and taking the rigid-spacetime limit, so that $\eta \rightarrow t$), we find

$$\begin{aligned} 0 &= \sum_{m=0}^{\infty} (-4m^2\omega^2 + k^2 + a_{k,0}) \alpha_{k,m} \cos 2m\omega t \\ &+ \sum_{m,n=1}^{\infty} a_{k,m} \alpha_{k,n} \cos 2m\omega t \cos 2n\omega t \\ &= \sum_{m=0}^{\infty} (-4m^2\omega^2 + k^2 + a_{k,0}) \alpha_{k,m} \cos 2m\omega t \\ &+ \sum_{m,n=1}^{\infty} \frac{a_{k,m} \alpha_{k,n}}{2} [\cos 2(m+n)\omega t + \cos 2(m-n)\omega t] \\ &= \sum_{p=0}^{\infty} \gamma_p \cos 2p\omega t, \end{aligned} \quad (\text{B2})$$

where the γ_p are linear combinations of the $\alpha_{k,m}$ coefficients. The boundaries of the stability regions for the modes v_k correspond to those places where each $\gamma_p = 0$. These correspond to the row of a matrix, U , whose vanishing determinant enforces the equation of motion of Eq. (22). The elements of the matrix U are given by

$$\begin{aligned} U_{00} &= k^2 + a_{k,0}, \\ U_{p,p} &= -4p^2\omega^2 + k^2 + a_{k,0} + \frac{a_{k,2p}}{2}, \quad p \geq 1, \\ U_{p,q} &= \frac{a_{k,|p-q|} + a_{k,p+q}}{2}, \quad p \neq q. \end{aligned} \quad (\text{B3})$$

The corresponding matrix for the isocurvature modes, z_k , which we will call Z , is given by simply replacing each a in the matrix above with b :

$$\begin{aligned} Z_{00} &= k^2 + b_{k,0}, \\ Z_{p,p} &= -4p^2\omega^2 + k^2 + b_{k,0} + \frac{b_{k,2p}}{2}, \quad p \geq 1, \\ Z_{p,q} &= \frac{b_{k,|p-q|} + b_{k,p+q}}{2}, \quad p \neq q. \end{aligned} \quad (\text{B4})$$

We may also expand v_k and z_k into their respective sine series:

$$v_k = \sum_{j=1}^{\infty} \alpha_{k,j} \sin 2j\omega t, \quad z_k = \sum_{j=1}^{\infty} \beta_{k,j} \sin 2j\omega t. \quad (\text{B5})$$

With these expansions, Eq. (22) becomes

$$\begin{aligned}
 0 &= \sum_{m=1}^{\infty} (-4m^2\omega^2 + k^2 + a_{k,0}) \alpha_{k,m} \sin 2m\omega t \\
 &+ \sum_{m,n=1}^{\infty} a_{k,m} \alpha_{k,n} \cos 2m\omega t \sin 2n\omega t \\
 &= \sum_{m=1}^{\infty} (-4m^2\omega^2 + k^2 + a_{k,0}) \alpha_{k,m} \sin 2m\omega t \\
 &+ \sum_{m,n=0}^{\infty} \frac{a_{k,m} \alpha_{k,n}}{2} [\sin 2(n+m)\omega t + \sin 2(n-m)\omega t] \\
 &= \sum_{p=1}^{\infty} \zeta_p \sin 2p\omega t.
 \end{aligned} \tag{B6}$$

Just as for the cosine expansion, we find a system of equations by setting each $\zeta_p = 0$. The matrix \mathcal{U} is given by

$$\begin{aligned}
 \mathcal{U}_{p,p} &= -4p^2\omega^2 + k^2 + a_{k,0} - \frac{a_{k,2p}}{2}, \quad p \geq 1, \\
 \mathcal{U}_{p,q} &= \frac{a_{k,|p-q|} + \text{sign}(q-p)a_{k,p+q}}{2}.
 \end{aligned} \tag{B7}$$

The corresponding matrix for the z_k 's is represented by the matrix \mathcal{Z} . The form of \mathcal{Z} is exactly the same as that of \mathcal{U} under the replacement of $a_{k,j}$ with $b_{k,j}$ for all j .

2. T -periodic solutions

We now consider the case in which v_k and z_k are T periodic. We can then make the following expansions:

$$v_k = \sum_{j=0}^{\infty} \alpha_{k,j} \cos j\omega t, \quad z_k = \sum_{j=0}^{\infty} \beta_{k,j} \cos j\omega t. \tag{B8}$$

Plugging these relations into Eq. (22), we find

$$\begin{aligned}
 0 &= \sum_{m=0}^{\infty} (-m^2\omega^2 + k^2 + a_{k,0}) \alpha_{k,m} \cos m\omega t \\
 &+ \sum_{m,n=1}^{\infty} a_{k,m} \alpha_{k,n} \cos 2m\omega t \cos n\omega t \\
 &= \sum_{m=0}^{\infty} (-m^2\omega^2 + k^2 + a_{k,0}) \alpha_{k,m} \cos m\omega t \\
 &+ \sum_{m,n=1}^{\infty} \frac{a_{k,m} \alpha_{k,n}}{2} [\cos(2m+n)\omega t + \cos(2m-n)\omega t] \\
 &= \sum_{p=0}^{\infty} \delta_p \cos 2p\omega t,
 \end{aligned} \tag{B9}$$

where δ_p are linear combinations of the $\alpha_{k,m}$ coefficients. Just as in the previous case, we form a matrix U' whose vanishing determinant yields equations for the boundaries of the stability bands for the adiabatic modes, v_k :

$$U'_{00} = k^2 + a_{k,0}, \tag{B10}$$

$$U'_{p,p} = -p^2\omega^2 + k^2 + a_{k,0} + \frac{a_{k,p}}{2}, \quad p \geq 1, \tag{B11}$$

$$U'_{p,q} = \frac{a_{k,|p-q|/2} + a_{k,(p+q)/2}}{2}, \quad p \neq q, \quad p \equiv q \pmod{2}. \tag{B12}$$

The corresponding matrix for z_k , which we call Z' , may be constructed by replacing $a_{k,j}$ with $b_{k,j}$ for all j .

We must also consider sine series with period T . After a similar procedure, we find the matrices of interest:

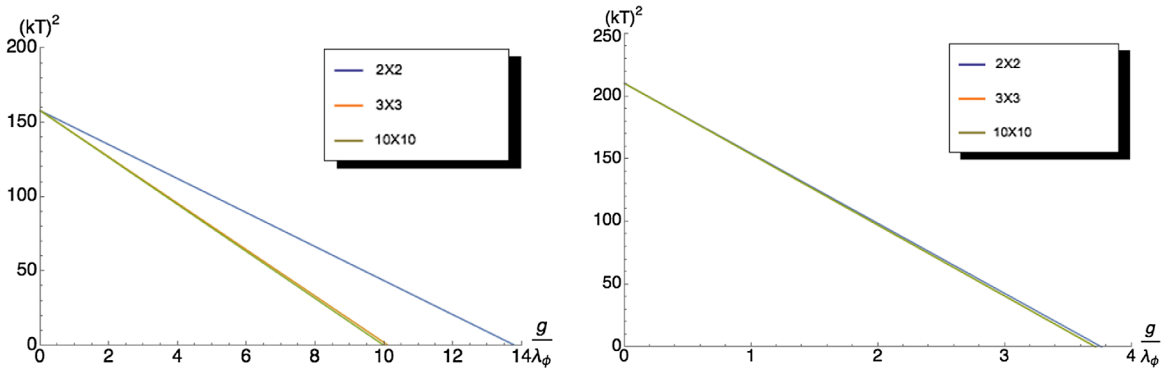


FIG. 23. Comparison of the stability boundary of the primary instability band given by $\det U = 0$ when U is truncated to 2×2 , 3×3 , and 10×10 matrices, for $\xi_\phi = 0$ (left) and $\xi_\phi = 0.5$ (right). All higher-dimension truncations are too close to the 10×10 truncation to resolve. Hence we find that the 3×3 truncation is sufficient to yield an accurate approximation to the location of the stability boundary in the $(kT)^2$ - (g/λ_ϕ) plane.

$$\mathcal{U}'_{p,p} = -p^2\omega^2 + k^2 + a_{k,0} - \frac{a_{k,p}}{2}, \quad p \geq 1,$$

$$\mathcal{U}'_{p,q} = \frac{a_{k,|p-q|/2} + \text{sign}(q-p)a_{k,(p+q)/2}}{2} \quad (\text{B13})$$

and the same for \mathcal{Z}' with $a_{k,j} \rightarrow b_{k,j}$.

To summarize, we construct eight distinct matrices: four U matrices for the adiabatic modes v_k (coming from the $T/2$ -periodic sine and cosine series and the T -periodic sine

and cosine series), and four Z matrices for the isocurvature modes z_k . Each of these matrices is a function of g/λ_ϕ and k . The vanishing of the determinants of these matrices determines the boundaries of the stability regions for the v_k and z_k modes in the $(kT)^2$ - (g/λ_ϕ) plane. Finally, in Fig. 23, we demonstrate that results of sufficient accuracy for the primary instability band may be calculated by truncating the infinite-dimensional matrices to simple 3×3 matrices.

-
- [1] M. P. DeCross, D. I. Kaiser, A. Prabhu, C. Prescod-Weinstein, and E. I. Sfakianakis, previous paper, Preheating after multifield inflation with nonminimal couplings. I. Covariant formalism and attractor behavior, *Phys. Rev. D* **97**, 023526 (2018).
 - [2] M. P. DeCross, D. I. Kaiser, A. Prabhu, C. Prescod-Weinstein, and E. I. Sfakianakis, following paper, Preheating after multifield inflation with nonminimal couplings. III. Dynamical spacetime results, *Phys. Rev. D* **97**, 023528 (2018).
 - [3] D. H. Lyth and A. Riotto, Particle physics models of inflation and the cosmological density perturbation, *Phys. Rep.* **314**, 1 (1999).
 - [4] D. Wands, Multiple field inflation, *Lect. Notes Phys.* **738**, 275 (2008).
 - [5] A. Mazumdar and J. Rocher, Particle physics models of inflation and curvaton scenarios, *Phys. Rep.* **497**, 85 (2011).
 - [6] J. Martin, C. Ringeval, and V. Vennin, Encyclopedia inflationaris, *Phys. Dark Universe* **5–6**, 75 (2014).
 - [7] V. Vennin, K. Koyama, and D. Wands, Encyclopedia curvatonis, *J. Cosmol. Astropart. Phys.* **11** (2015) 008.
 - [8] J.-O. Gong, Multi-field inflation and cosmological perturbations, *Int. J. Mod. Phys. D* **26**, 1740003 (2017).
 - [9] C. G. Callan, Jr., S. R. Coleman, and R. Jackiw, A new improved energy-momentum tensor, *Ann. Phys. (N.Y.)* **59**, 42 (1970).
 - [10] T. S. Bunch, P. Panangaden, and L. Parker, On renormalization of $\lambda\phi^4$ field theory in curved space-time. I, *J. Phys. A* **13**, 901 (1980); T. S. Bunch and P. Panangaden, On renormalization of $\lambda\phi^4$ field theory in curved space-time. II, *J. Phys. A* **13**, 919 (1980).
 - [11] N. D. Birrell and P. C. W. Davies, *Quantum Fields in Curved Space* (Cambridge University Press, New York, 1982).
 - [12] I. L. Buchbinder, S. D. Odintsov, and I. L. Shapiro, *Effective Action in Quantum Gravity* (Taylor and Francis, New York, 1992).
 - [13] L. E. Parker and D. J. Toms, *Quantum Field Theory in Curved Spacetime* (Cambridge University Press, New York, 2009).
 - [14] S. D. Odintsov, Renormalization group, effective action, and grand unification theories in curved spacetime, *Fortschr. Phys.* **39**, 621 (1991).
 - [15] T. Markkanen and A. Tranberg, A simple method for one-loop renormalization in curved spacetime, *J. Cosmol. Astropart. Phys.* **08** (2013) 045.
 - [16] F. L. Bezrukov and M. E. Shaposhnikov, The Standard Model Higgs boson as the inflaton, *Phys. Lett. B* **659**, 703 (2008).
 - [17] T. Futamase and K. Maeda, Chaotic inflationary scenario of the Universe with a nonminimally coupled “inflaton” field, *Phys. Rev. D* **39**, 399 (1989).
 - [18] D. S. Salopek, J. R. Bond, and J. M. Bardeen, Designing density fluctuation spectra in inflation, *Phys. Rev. D* **40**, 1753 (1989).
 - [19] R. Fakir, S. Habib, and W. G. Unruh, Cosmological density perturbations with modified gravity, *Astrophys. J.* **394**, 396 (1992); R. Fakir and W. G. Unruh, Improvement on cosmological chaotic inflation through nonminimal coupling, *Phys. Rev. D* **41**, 1783 (1990).
 - [20] N. Makino and M. Sasaki, The density perturbation in the chaotic inflation with nonminimal coupling, *Prog. Theor. Phys.* **86**, 103 (1991).
 - [21] D. I. Kaiser, Constraints in the context of induced gravity inflation, *Phys. Rev. D* **49**, 6347 (1994).
 - [22] D. I. Kaiser, Primordial spectral indices from generalized Einstein theories, *Phys. Rev. D* **52**, 4295 (1995).
 - [23] D. I. Kaiser, E. A. Mazenc, and E. I. Sfakianakis, Primordial bispectrum from multifield inflation with nonminimal couplings, *Phys. Rev. D* **87**, 064004 (2013).
 - [24] R. N. Greenwood, D. I. Kaiser, and E. I. Sfakianakis, Multifield dynamics of Higgs inflation, *Phys. Rev. D* **87**, 064021 (2013).
 - [25] D. I. Kaiser and E. I. Sfakianakis, Multifield Inflation after Planck: The Case for Nonminimal Couplings, *Phys. Rev. Lett.* **112**, 011302 (2014).
 - [26] K. Schutz, E. I. Sfakianakis, and D. I. Kaiser, Multifield inflation after Planck: Isocurvature modes from nonminimal couplings, *Phys. Rev. D* **89**, 064044 (2014).
 - [27] R. Kallosh and A. Linde, Non-minimal inflationary attractors, *J. Cosmol. Astropart. Phys.* **10** (2013) 033; Multi-field conformal cosmological attractors, *J. Cosmol. Astropart. Phys.* **12** (2013) 006; R. Kallosh, A. Linde, and D. Roest, Universal Attractor for Inflation at Strong Coupling, *Phys. Rev. Lett.* **112**, 011303 (2014); R. Kallosh, A. Linde, and D. Roest, Superconformal inflationary α -attractors, *J. High Energy Phys.* **11** (2013) 198;

- M. Galante, R. Kallosh, A. Linde, and D. Roest, Unity of Cosmological Attractors, *Phys. Rev. Lett.* **114**, 141302 (2015); R. Kallosh and A. Linde, Planck, LHC, and α -attractors, *Phys. Rev. D* **91**, 083528 (2015); J. J. M. Carrasco, R. Kallosh, and A. Linde, Cosmological attractors and initial conditions for inflation, *Phys. Rev. D* **92**, 063519 (2015).
- [28] A. H. Guth and D. I. Kaiser, Inflationary cosmology: Exploring the universe from the smallest to the largest scales, *Science* **307**, 884 (2005).
- [29] B. A. Bassett, S. Tsujikawa, and D. Wands, Inflation dynamics and reheating, *Rev. Mod. Phys.* **78**, 537 (2006).
- [30] R. Allahverdi, R. Brandenberger, F.-Y. Cyr-Racine, and A. Mazumdar, Reheating in inflationary cosmology: Theory and applications, *Annu. Rev. Nucl. Part. Sci.* **60**, 27 (2010).
- [31] A. V. Frolov, Non-linear dynamics and primordial curvature perturbations from preheating, *Classical Quantum Gravity* **27**, 124006 (2010).
- [32] M. A. Amin, M. P. Hertzberg, D. I. Kaiser, and J. Karouby, Nonperturbative dynamics of reheating after inflation: A review, *Int. J. Mod. Phys. D* **24**, 1530003 (2015).
- [33] M. A. Amin and D. Baumann, From wires to cosmology, *J. Cosmol. Astropart. Phys.* **02** (2016) 045.
- [34] P. Adshead, R. Easther, J. Pritchard, and A. Loeb, Inflation and the scale dependent spectral index: Prospects and strategies, *J. Cosmol. Astropart. Phys.* **02** (2011) 021.
- [35] L. Dai, M. Kamionkowski, and J. Wang, Reheating Constraints to Inflationary Models, *Phys. Rev. Lett.* **113**, 041302 (2014).
- [36] P. Creminelli, D. L. Nacir, M. Simonovi, G. Trevisan, and M. Zaldarriaga, φ^2 inflation at its endpoint, *Phys. Rev. D* **90**, 083513 (2014).
- [37] J. Martin, C. Ringeval, and V. Vennin, Observing the Inflationary Reheating, *Phys. Rev. Lett.* **114**, 081303 (2015).
- [38] J.-O. Gong, G. Leung, and S. Pi, Probing reheating with primordial spectrum, *J. Cosmol. Astropart. Phys.* **05** (2015) 027.
- [39] R.-G. Cai, Z.-K. Guo, and S.-J. Wang, Reheating phase diagram for single-field slow-roll inflationary models, *Phys. Rev. D* **92**, 063506 (2015).
- [40] J. L. Cook, E. Dimastrogiovanni, D. A. Easson, and L. M. Krauss, Reheating predictions in single field inflation, *J. Cosmol. Astropart. Phys.* **04** (2015) 047.
- [41] V. Domcke and J. Heisig, Constraints on the reheating temperature from sizable tensor modes, *Phys. Rev. D* **92**, 103515 (2015).
- [42] L. Kofman, A. Linde, and A. Starobinsky, Towards the theory of reheating after inflation, *Phys. Rev. D* **56**, 3258 (1997).
- [43] P. B. Greene and L. Kofman, Preheating of fermions, *Phys. Lett. B* **448**, 6 (1999); P. B. Greene and L. Kofman, On the theory of fermionic preheating, *Phys. Rev. D* **62**, 123516 (2000).
- [44] M. Peloso and L. Sorbo, Preheating of massive fermions after inflation: Analytical results, *J. High Energy Phys.* **05** (2000) 016.
- [45] S. Tsujikawa, B. A. Bassett, and F. Viniegra, Multi-field fermionic preheating, *J. High Energy Phys.* **08** (2000) 019.
- [46] A. L. Maroto and A. Mazumdar, Production of Spin 3/2 Particles from Vacuum Fluctuations, *Phys. Rev. Lett.* **84**, 1655 (2000).
- [47] R. Kallosh, L. Kofman, A. D. Linde, and A. Van Proeyen, Gravitino production after inflation, *Phys. Rev. D* **61**, 103503 (2000).
- [48] A.-C. Davis, K. Dimopoulos, T. Prokopec, and O. Tornkvist, Primordial spectrum of gauge fields from inflation, *Phys. Lett. B* **501**, 165 (2001).
- [49] J. García-Bellido, M. Garcia-Perez, and A. Gonzalez-Arroyo, Chern-Simons production during preheating in hybrid inflation models, *Phys. Rev. D* **69**, 023504 (2004).
- [50] F. Bezrukov, D. Gorbunov, and M. Shaposhnikov, On initial conditions for the hot big bang, *J. Cosmol. Astropart. Phys.* **06** (2009) 029.
- [51] J. García-Bellido, D. G. Figueroa, and J. Rubio, Preheating in the Standard Model with the Higgs-inflaton coupled to gravity, *Phys. Rev. D* **79**, 063531 (2009).
- [52] J.-F. Dufaux, D. G. Figueroa, and J. García-Bellido, Gravitational waves from Abelian gauge fields and cosmic strings at preheating, *Phys. Rev. D* **82**, 083518 (2010).
- [53] M. A. Amin, R. Easther, and H. Finkel, Inflaton fragmentation and oscillon formation in three dimensions, *J. Cosmol. Astropart. Phys.* **12** (2010) 001; M. A. Amin, R. Easther, H. Finkel, R. Flauger, and H. P. Hertzberg, Oscillons after Inflation, *Phys. Rev. Lett.* **108**, 241302 (2012).
- [54] S.-Y. Zhou, E. J. Copeland, R. Easther, H. Finkel, Z.-G. Mou, and P. M. Saffin, Gravitational waves from oscillon preheating, *J. High Energy Phys.* **10** (2013) 026; S.-Y. Zhou, Gravitational waves from Affleck-Dine condensate fragmentation, *J. Cosmol. Astropart. Phys.* **06** (2015) 033.
- [55] R. Allahverdi, A. Ferrantelli, J. Garcia-Bellido, and A. Mazumdar, Non-perturbative production of matter and rapid thermalization after MSSM inflation, *Phys. Rev. D* **83**, 123507 (2011).
- [56] J. García-Bellido, J. Rubio, and M. Shaposhnikov, Higgs-dilaton cosmology: Are there extra relativistic species?, *Phys. Lett. B* **718**, 507 (2012).
- [57] J. T. Deskins, J. T. Giblin, and R. R. Caldwell, Gauge field preheating at the end of inflation, *Phys. Rev. D* **88**, 063530 (2013).
- [58] M. P. Hertzberg and J. Karouby, Baryogenesis from the inflaton field, *Phys. Lett. B* **737**, 34 (2014); M. P. Hertzberg and J. Karouby, Generating the observed baryon asymmetry from the inflaton field, *Phys. Rev. D* **89**, 063523 (2014).
- [59] K. D. Lozanov and M. A. Amin, End of inflation, oscillons, and matter-antimatter asymmetry, *Phys. Rev. D* **90**, 083528 (2014).
- [60] M. P. Hertzberg, J. Karouby, W. G. Spitzer, J. C. Becerra, and L. Li, A theory of self-resonance after inflation. I. Adiabatic and isocurvature Goldstone modes, *Phys. Rev. D* **90**, 123528 (2014); M. P. Hertzberg, J. Karouby, W. G. Spitzer, J. C. Becerra, and L. Li, A theory of self-resonance after inflation. II. Quantum mechanics and particle-antiparticle asymmetry, *Phys. Rev. D* **90**, 123529 (2014).
- [61] P. Adshead and E. I. Sfakianakis, Fermion production during and after axion inflation, *J. Cosmol. Astropart. Phys.* **11** (2015) 021.

- [62] P. Adshead, J. T. Giblin, T. R. Scully, and E. I. Sfakianakis, Gauge-preheating and the end of axion inflation, *J. Cosmol. Astropart. Phys.* **12** (2015) 034; P. Adshead, J. T. Giblin, T. R. Scully, and E. I. Sfakianakis, Magnetogenesis from axion inflation, *J. Cosmol. Astropart. Phys.* **10** (2016) 039.
- [63] P. Adshead and E. I. Sfakianakis, Leptogenesis from Left-Handed Neutrino Production during Axion Inflation, *Phys. Rev. Lett.* **116**, 091301 (2016).
- [64] E. McDonough, H. B. Moghaddam, and R. H. Brandenberger, Preheating and entropy perturbations in axion monodromy inflation, *J. Cosmol. Astropart. Phys.* **05** (2016) 012.
- [65] M. A. Amin and D. Baumann, From wires to cosmology, *J. Cosmol. Astropart. Phys.* **02** (2016) 045.
- [66] K. D. Lozanov and M. A. Amin, The charged inflaton and its gauge fields: Preheating and initial conditions for reheating, *J. Cosmol. Astropart. Phys.* **06** (2016) 032.
- [67] K. D. Lozanov and M. A. Amin, Equation of State and Duration to Radiation Domination after Inflation, *Phys. Rev. Lett.* **119**, 061301 (2017).
- [68] D. G. Figueroa and F. Torrenti, Parametric resonance in the early universe: A fitting analysis, *J. Cosmol. Astropart. Phys.* **02** (2017) 001.
- [69] B. A. Bassett and S. Liberati, Geometric reheating after inflation, *Phys. Rev. D* **58**, 021302 (1998).
- [70] S. Tsujikawa, K. Maeda, and T. Torii, Resonant particle production with nonminimally coupled scalar fields in preheating after inflation, *Phys. Rev. D* **60**, 063515 (1999); S. Tsujikawa, K. Maeda, and T. Torii, Preheating with nonminimally coupled scalar fields in higher-curvature inflation models, *Phys. Rev. D* **60**, 123505 (1999); S. Tsujikawa, K. Maeda, and T. Torii, Preheating of the nonminimally coupled inflaton field, *Phys. Rev. D* **61**, 103501 (2000).
- [71] S. Tsujikawa and B. A. Bassett, A new twist to preheating, *Phys. Rev. D* **62**, 043510 (2000); S. Tsujikawa and B. A. Bassett, When can preheating affect the CMB?, *Phys. Lett. B* **536**, 9 (2002).
- [72] Y. Watanabe and J. White, Multifield formulation of gravitational particle production after inflation, *Phys. Rev. D* **92**, 023504 (2015).
- [73] J. Lachapelle and R. H. Brandenberger, Preheating with non-standard kinetic term, *J. Cosmol. Astropart. Phys.* **04** (2009) 020.
- [74] J. Karouby, B. Underwood, and A. C. Vincent, Preheating with the brakes on: The effects of a speed limit, *Phys. Rev. D* **84**, 043528 (2011).
- [75] H. L. Child, J. T. Giblin, Jr., R. Ribeiro, and D. Seery, Preheating with Nonminimal Kinetic Terms, *Phys. Rev. Lett.* **111**, 051301 (2013).
- [76] J. Zhang, Y. Cai, and Y.-S. Piao, Preheating in a DBI inflation model, [arXiv:1307.6529](https://arxiv.org/abs/1307.6529).
- [77] K. Kannike, G. Hütsi, L. Pizza, A. Racioppi, M. Raidal, A. Salvio, and A. Strumia, Dynamically induced Planck scale and inflation, *J. High Energy Phys.* **05** (2015) 065; K. Kannike, A. Racioppi, and M. Raidal, Linear inflation from quartic potential, *J. High Energy Phys.* **01** (2016) 035.
- [78] C. van de Bruck, P. Dunsby, and L. E. Paduraru, Reheating and preheating in the simplest extension of Starobinsky inflation, *Int. J. Mod. Phys. D* **26**, 1750152 (2017).
- [79] Y. Ema, R. Jinno, K. Mukaida, and K. Nakayama, Violent preheating in inflation with nonminimal coupling, *J. Cosmol. Astropart. Phys.* **02** (2017) 045.
- [80] N. Barnaby, J. Braden, and L. Kofman, Reheating the universe after multi-field inflation, *J. Cosmol. Astropart. Phys.* **07** (2010) 016.
- [81] D. Battefeld and S. Kawai, Preheating after N-flation, *Phys. Rev. D* **77**, 123507 (2008); D. Battefeld, Preheating after multifield inflation, *Nucl. Phys. B, Proc. Suppl.* **192–193**, 126 (2009); D. Battefeld, T. Battefeld, and J. T. Giblin, Jr., On the suppression of parametric resonance and the viability of tachyonic preheating after multifield inflation, *Phys. Rev. D* **79**, 123510 (2009); T. Battefeld, A. Eggemeier, and J. T. Giblin, Jr., Enhanced preheating after multifield inflation: On the importance of being special, *J. Cosmol. Astropart. Phys.* **11** (2012) 062.
- [82] D. I. Kaiser, Conformal transformations with multiple scalar fields, *Phys. Rev. D* **81**, 084044 (2010).
- [83] H. Abedi and A. M. Abbassi, Gravitational constant in multiple field gravity, *J. Cosmol. Astropart. Phys.* **05** (2015) 026.
- [84] D. Boyanovsky, H. J. de Vega, R. Holman, and J. Salgado, Analytic and numerical study of preheating dynamics, *Phys. Rev. D* **54**, 7570 (1996).
- [85] D. I. Kaiser, Preheating in an expanding universe: Analytic results for the massless case, *Phys. Rev. D* **56**, 706 (1997); D. I. Kaiser, Resonance structure for preheating with massless fields, *Phys. Rev. D* **57**, 702 (1998).
- [86] P. Greene, L. Kofman, A. Linde, and A. Starobinsky, Structure of resonance in preheating after inflation, *Phys. Rev. D* **56**, 6175 (1997).
- [87] A. O. Barvinsky, A. Yu. Kamenshik, C. Kiefer, A. A. Starobinsky, and C. F. Steinwachs, Asymptotic freedom in inflationary cosmology with a nonminimally coupled Higgs field, *J. Cosmol. Astropart. Phys.* **12** (2009) 003; A. O. Barvinsky, A. Yu. Kamenshik, C. Kiefer, A. A. Starobinsky, and C. F. Steinwachs, Higgs boson, renormalization group, and naturalness in cosmology, *Eur. Phys. J. C* **72**, 2219 (2012).
- [88] F. Bezrukov, A. Magnin, M. Shaposhnikov, and S. Sibiryakov, Higgs inflation: Consistency and generalisations, *J. High Energy Phys.* **01** (2011) 016; F. Bezrukov, M. Yu. Kalmykov, B. A. Kniehl, and M. E. Shaposhnikov, Higgs boson mass and new physics, *J. High Energy Phys.* **10** (2012) 140; F. Bezrukov, The Higgs field as an inflaton, *Classical Quantum Gravity* **30**, 214001 (2013).
- [89] K. Allison, Higgs ξ -inflation for the 125–126 GeV Higgs: A two-loop analysis, *J. High Energy Phys.* **02** (2014) 040.
- [90] I. G. Moss, Vacuum stability and the scaling behaviour of the Higgs-curvature coupling, [arXiv:1509.03554](https://arxiv.org/abs/1509.03554).
- [91] S. Renaux-Petel and K. Turzynski, On reaching the adiabatic limit in multi-field inflation, *J. Cosmol. Astropart. Phys.* **06** (2015) 010.
- [92] D. I. Kaiser, Post-inflation reheating in an expanding universe, *Phys. Rev. D* **53**, 1776 (1996).
- [93] *Handbook of Mathematical Functions*, edited by M. Abramowitz and I. Stegun (Dover, New York, 1965).
- [94] A. Taruya and Y. Nambu, Cosmological perturbation with two scalar fields in reheating after inflation, *Phys. Lett. B* **428**, 37 (1998).

- [95] B. A. Bassett, D. I. Kaiser, and R. Maartens, General relativistic effects in preheating, *Phys. Lett. B* **455**, 84 (1999).
- [96] B. A. Bassett, F. Tamburini, D. I. Kaiser, and R. Maartens, Metric preheating and limitations of linearized gravity, *Nucl. Phys.* **B561**, 188 (1999).
- [97] B. A. Bassett, C. Gordon, R. Maartens, and D. I. Kaiser, Restoring the sting to metric preheating, *Phys. Rev. D* **61**, 061302 (2000).
- [98] F. Finelli and R. Brandenberger, Parametric amplification of metric fluctuations during reheating in two field models, *Phys. Rev. D* **62**, 083502 (2000).
- [99] A. Chambers and A. Rajantie, Lattice Calculation of Non-Gaussianity from Preheating, *Phys. Rev. Lett.* **100**, 041302 (2008).
- [100] J. R. Bond, A. V. Frolov, Z. Huang, and L. Kofman, Non-Gaussian Spikes from Chaotic Billiards in Inflation Preheating, *Phys. Rev. Lett.* **103**, 071301 (2009).
- [101] L. Bethke, D. G. Figueroa, and A. Rajantie, Anisotropies in the Gravitational Wave Background from Preheating, *Phys. Rev. Lett.* **111**, 011301 (2013).
- [102] H. B. Moghaddam, R. H. Brandenberger, Y.-F. Cai, and E. G. M. Ferreira, Parametric resonance of entropy perturbations in massless preheating, *Int. J. Mod. Phys. D* **24**, 1550082 (2015).
- [103] Note that the definition of the ellipticity is defined globally for the system, regardless of the fields' trajectory through field space. This means that for a field trajectory along $\phi = 0$, the effects for positive and negative ellipticity will be inverted, compared to Fig. 22.